The epitranscriptomic m6A RNA modification modulates synaptic function in ageing and in a mouse model of synucleinopathy

Avika Chopra[1], Mary Xylaki[1,2], Fanzheng Yin[1], Ricardo Castro-Hernández[3], Madiha Merghani[1], Valentina Grande[1], Brit Mollenhauer[2,4], André Fischer[3,5,6], and Tiago F. Outeiro[1,7,8,9*]

1. University Medical Center Göttingen, Department of Experimental Neurodegeneration, Center for Biostructural Imaging of Neurodegeneration, 37073, Göttingen, Germany.
2. Department of Neurology, University Medical Centre Göttingen, 37073, Göttingen, Germany.
3. Department for Systems Medicine and Epigenetics, German Center for Neurodegenerative Diseases (DZNE), Göttingen, Germany
4. Paracelsus Elena Klinik, Kassel, Germany
5. Department of Psychiatry and Psychotherapy, University Medical Center Göttingen, Göttingen, Germany
6. Cluster of Excellence "Multiscale Bioimaging: from Molecular Machines to Networks of Excitable Cells" (MBExC), University of Göttingen, Germany
7. Max Planck Institute for Multidisciplinary Sciences, 37075 Göttingen, Germany.
8. Translational and Clinical Research Institute, Faculty of Medical Sciences, Newcastle University, Framlington Place, Newcastle Upon Tyne, NE2 4HH, UK.
9. Scientific employee with an honorary contract at Deutsches Zentrum für Neurodegenerative Erkrankungen (DZNE), 37075, Göttingen, Germany.

***Correspondence to:** Tiago F. Outeiro

Department of Experimental Neurodegeneration, Centre for Biostructural Imaging of Neurodegeneration, University Medical Centre Göttingen, Göttingen, Germany

Email: tiago.outeiro@med.uni-goettingen.de

Abstract

N6-methyladenosine (m6A) is the most abundant and conserved transcriptional modification in eukaryotic RNA, regulating RNA fate. While the functions of m6A in the development of the mammalian brain have been extensively studied, its roles in synaptic plasticity, cognitive decline, motor function, or other brain circuits remain underexplored. To date, the role of this modification in Parkinson's disease (PD) and other synucleinopathies has been largely unknown. Here, we investigated the m6A epitranscriptome in a mouse model of synucleinopathy. We performed m6A RNA immunoprecipitation sequencing (meRIP-seq) to obtain the m6A epitranscriptome of the midbrain in young (3 mo) and aged (15 mo) A30P-aSyn transgenic mice (aSyn Tg) and C57BL6 control wild type (Wt) mice. We observed hypermethylation of synaptic genes in 3 mo aSyn Tg mice compared to age-matched Wt mice. This methylation was reduced during ageing, with synaptic genes becoming increasingly hypomethylated. Using immunofluorescence imaging alongside biochemical analysis, we further investigated the expression of m6A regulatory enzymes — writer, N6-Adenosine-Methyltransferase Complex Catalytic Subunit (METTL3); reader, YTH N6-methyladenosine RNA-binding protein (YTHDF1); and eraser, fat mass and obesity-associated protein (FTO) — in the cortex, striatum, hippocampus, and cerebellum of Wt and aSyn Tg mice, as well as in primary cortical neuronal cultures. We observed that the levels of METTL3, YTHDF1 and FTO were similar between Wt and aSyn Tg mice. Interestingly, the writer protein METTL3 was found in both the nucleus and in the post-synaptic compartment in neuronal cultures. Our findings suggest that alterations in the regulation of m6A RNA methylation may be associated with

neurodegeneration and ageing and that this level of epitranscriptomic regulation plays a significant role at the synapse.

Keywords: epigenetics, m6A, Parkinson's disease, ageing, METTL3

54 # Introduction

55 Epigenetics is a process that acts as a bridge between genotype and phenotype, changing
56 the outcome of a gene without modifying the DNA sequence. It encompasses various types
57 of alterations such as methylation of DNA, histone modifications, and chromatin remodeling
58 [1,2]. The field that studies posttranscriptional changes of RNA bases is known as
59 epitranscriptomics and aims to identify modifications in the transcriptome and unravel their
60 regulatory roles [3]. N^6-methyladenine (m6A) modification is the most prevalent mRNA
61 modification occurring at a frequency of 0.15 - 0.6% of all adenosines [4–6] and is found in
62 different types of RNAs including protein coding, messenger RNA (mRNA) [7,8]. This
63 modification is being heavily studied due to its prevalence and importance in eukaryotes,
64 where it regulates various cellular functions [8–12]. Methylation marks are mostly added co-
65 transcriptionally to specific consensus motif sequences and are mostly found close to the 3'
66 un-translated region (3'-UTR) at the stop codon [4,13].

67 The m6A modification machinery consists of three groups of enzymes, namely
68 methyltransferases, demethylases and detectors of this modification, also termed writers,
69 erasers, and readers, respectively. The modification can be added onto the RNA by
70 methyltransferases including methyltransferase-like 3 (METTL3), methyltransferase-like 14
71 (METTL14), and adapter protein Wilms tumour 1-associated protein (WTAP) [5,14–19].
72 METTL3 was the first discovered methyltransferase and was described as a key component
73 in the methylation of transcripts involved in physiological processes such as embryonic
74 development and brain development [20–23]. The catalytically active part of METTL3 forms
75 a heterodimer with METTL14, which provides the structure to install the m6A modification
76 onto RNA [5,24–27]. Apart from these, the m6A methyltransferase complex comprises other

77 proteins, including RNA binding proteins (RBP) like RBP15, which recruit this machinery to
78 the target mRNA to facilitate methylation [15,28]. Demethylases, for instance, fat mass and
79 obesity-associated protein (FTO) and alkB homologue 5 (ALKBH5) remove the m6A
80 modification marks making this a dynamic process [29,30]. FTO was the first eraser protein
81 identified [29,31] and it carries out oxidative demethylation where m6A is converted in
82 several steps to N^6-hydroxymethyl adenosine (hm6A), then to N^6-formyladenosine (f6A) and
83 lastly to adenine [31]. Additionally, reader proteins like the YT521-B homology (YTH)
84 domain family of proteins including YTHDF1, YTHDF2/3, insulin-like growth factor 2 mRNA-
85 binding proteins (IGF2BP1), heterogeneous nuclear ribonucleoprotein (HNRNPA2B1)
86 recognise the modification and modulate alternative splicing and processing of target
87 transcripts [8,32]. The ones located in the cytoplasm include YTHDF1, YTHDF2, and YTHDF3.
88 The main function of these proteins is unclear; however, studies indicate different roles of
89 these enzymes in a cell. While YTHDF1 promotes the translation of mRNA thereby
90 promoting its protein expression, YTHDF2 promotes the degradation of mRNA, and YTHDF3
91 promotes both translation and degradation of mRNA [33,34].

92 m6A methylation has been associated with ageing, and downregulation in the expression of
93 FTO and an overall increase in RNA m6A modification was found in human follicular fluid
94 (FF) and granulosa cells (GCs) from aged donors and murine ovaries from old mice [35].
95 Another recent study has also highlighted the relationship between elevated m6A levels and
96 brain ageing in both mice and humans [36], although a significant downregulation of m6A
97 methylation in ageing mice and in postmortem brain tissue from Alzheimer's disease
98 patients has also been reported [37].

99 Strikingly, ageing is also a major risk factor for the onset and progression of
100 neurodegenerative disorders such as Parkinson's disease (PD) and related
101 synucleinopathies, disorders associated with the accumulation of aggregated alpha-
102 synuclein (aSyn) protein in the brain. Despite the growing interest in the role of m6A
103 methylation in ageing, its role in PD is still unclear and remains controversial. While a recent
104 study indicated that the expression levels of m6A are significantly reduced in cellular models
105 of PD and in the striatum of a rodent model of PD [38], a different study showed that the
106 m6A methyl transferases were significantly decreased while the demethylases were
107 increased in the substantia nigra and in the striatum of mouse models of PD [39]. Ageing
108 also affects multiple homeostatic pathways including mitochondrial function and protein
109 degradation pathways, ultimately leading to cell death in the substantia nigra [40–42].

110 In this study, we investigated the m6A RNA modification profile in the context of ageing and
111 neurodegeneration in a mouse model of synucleinopathy. We performed methylated RNA
112 immunoprecipitation sequencing (meRIP-seq) to obtain the m6A epitranscriptome of the
113 midbrain of C57BL6 (Wt) control and A30P aSyn PD (aSyn Tg) mice at 3 months (3 mo) and
114 15 months (15 mo) of age. We observed an increase in the m6A methylation in the genes
115 involved in the molecular and biological processes at the synapse. Several genes involved in
116 synaptic processes were hypermethylated in 3 mo aSyn Tg vs. Wt mice, while the
117 methylation marks were reduced in 15 mo aSyn Tg vs. age-matched Wt mice. Using
118 immunofluorescence imaging of primary cortical neurons, we observed that the localisation
119 of the writer METTL3 enzyme is not only limited to the nucleus but is also present at the
120 post-synapse. Our findings suggest that m6A RNA methylation is possibly playing a role in
121 neurodegeneration and ageing, and is involved in regulating synaptic function.

122

123 # Results

124 **m6A alterations during ageing in Wt mice and in a transgenic model of synucleinopathy**

125 We began by examining the distribution of differentially expressed transcripts and
126 transcripts with m6A methylation in the healthy ageing brain of Wt mice. We further
127 extended the analysis to aSyn Tg mice, in order to compare the effects of ageing on m6A
128 modification and assess this change in the context of synucleinopathy. We extracted and
129 dissected the midbrains from five 3 mo and five 15 mo Wt and an equal number of aSyn Tg
130 mice, as this brain region is particularly relevant in the context of PD and related
131 synucleinopathies. Methylated RNA immunoprecipitation sequencing (meRIP-seq) was
132 performed to determine the midbrain-specific epitranscriptomic landscape in 3 mo and 15
133 mo mice (Figure 1A, B). First, we compared the differential expression of genes due to
134 ageing in 15 mo vs 3 mo mice in both Wt and aSyn Tg animals. We observed a stronger
135 effect in aSyn Tg mice where 270 transcripts were differentially expressed when compared
136 with Wt mice, where only 79 transcripts were differentially expressed. Most differentially
137 expressed transcripts in aSyn Tg mice were downregulated (Supplementary Figure S1C).
138 However, when we compared the differentially methylated transcripts, we found similar
139 numbers between Wt (420 genes) and Tg (424 genes) mice (Figure 1A).

140 On the other hand, the effect of aSyn A30P overexpression was assessed by a comparison
141 between aSyn Tg and Wt mice at 3 mo and 15 mo. We did not identify major differences in
142 the number of differentially expressed transcripts which were 128 at 3 mo and 142 at 15
143 mo. Similarly, the differentially methylated transcripts showed no significant changes

144 between Wt and aSyn Tg at 3 mo (384 genes) and 15 mo (353 genes) (Figure 1B). While we
145 did not see a significant difference in the differential methylation, we found that the
146 prevalence of hyper- and hypomethylated transcripts was reversed (Figure 1B).

147 As a consequence of ageing, the methylation levels of the differentially methylated m6A
148 transcripts in 15 mo vs. 3 mo Wt mice we found 418 hypermethylated and only 2
149 hypomethylated transcripts. On the contrary, 171 genes were hypermethylated and 244
150 transcripts were hypomethylated in 15 mo vs. 3 mo aSyn Tg mice (Figure 1D). A transcript
151 can carry multiple m6A methylation marks and some of these marks likely increase while
152 others decrease simultaneously. Such transcripts are referred to as mixed transcripts. We
153 found only 9 such mixed transcripts (Figure 1D, left column) in aSyn Tg mice during ageing.

154 To identify the effect of aSyn expression on the levels of the m6A modification, we
155 compared 3 mo aSyn Tg mice with age-matched Wt mice. We found 380 hypermethylated
156 transcripts and only 4 transcripts were hypomethylated, and no mixed transcripts. On the
157 other hand, when comparing 15 mo aSyn Tg vs. Wt mice, a reverse trend was observed,
158 with 108 hypermethylated, 240 hypomethylated, and only 5 mixed transcripts (Figure 1D,
159 right column).

160 We found 6135 methylated transcripts in common between all groups (Figure 1E). The 3 mo
161 Wt mice displayed 266 unique methylated transcripts and the 15 mo Wt mice 255. These
162 numbers were lower for the aSyn Tg group where the 3 mo mice showed 165 unique
163 methylated transcripts and the 15 mo mice showed 189. At 15 months, both genotypes
164 showed 124 commonly methylated transcripts, suggesting the occurrence of conserved

165 processes in normal ageing and synucleinopathies. The aSyn Tg mice displayed 53
166 methylated transcripts correlated with aSyn expression and conserved with ageing.

167 The overall distribution of m6A methylation peaks on mRNA did not display any striking
168 anomalies in any of the groups. As expected, the majority of the m6A modifications were
169 localised close to the 3' UTR on mRNA (Figure 1F), as previously reported for ageing-related
170 genes [36].

171

172 **m6A levels are reduced in synaptic transcripts upon ageing**

173 To investigate the cellular processes and the subcellular regions where the differentially
174 methylated transcripts were identified in 15 mo aSyn Tg vs. Wt mice, we performed gene
175 ontology (GO) term analysis. We found that synaptic function was the biological process
176 most represented. Our analysis revealed that transcripts with m6A methylation marks have
177 strong enrichment for biological processes such as receptor internalization, excitatory post-
178 synaptic potential, axonal transport, and dendritic spine morphogenesis. The identified
179 transcripts were also involved in cellular processes including neuron projection cytoplasm
180 and synaptic vesicle membrane (Figure 2A). Previous data from our group has also shown
181 that while the average dendritic spine number was not significantly different, a strong
182 difference was observed in the abundance of different types of spines in aSyn Tg neurons
183 when compared with Wt neurons [67].

184 We also observed that when we compared the differentially enriched genes in aSyn Tg 15
185 mo vs. 3 mo, we saw a strong enrichment of pathways involved in the immune system. The

186 genes with highest enrichment score were involved in innate immune system, adaptive
187 immune system, immunoglobulin binding, phagocytic vesicle, defense response, innate
188 immune response, and regulation of immune system processes among others
189 (Supplementary Figure S2).

190 We used the SynGO software [64] (https://syngoportal.org/), an experimentally annotated
191 database for synaptic location and functional GO, to specifically check the m6A methylation
192 of synaptic transcripts. These differentially methylated genes are primarily involved in
193 synaptic organisation, metabolism, transport, signaling, and both pre-and post-synaptic
194 processes. Based on meRIP and RNA sequencing analysis, sunburst plots of Wt and aSyn Tg
195 mice were generated (Figure 2B). Our findings suggest that the differentially methylated
196 transcripts that are involved at the synapse and in synaptic function were majorly
197 hypermethylated in 3 mo aSyn Tg mice compared to 3 mo Wt mice (Figure 2A). In 3 mo
198 mice, the hypermethylated transcripts were concentrated in synapse organisation and at
199 the pre-synapse (Figure 2B). Conversely, at 15 months of age, the majority of the
200 differentially methylated transcripts were hypomethylated when aSyn Tg mice are
201 compared with Wt mice, which were largely involved in signalling, pre- and post-synapse,
202 and synapse organisation (Figure 2C).

203 In summary, we observed that the differentially methylated genes, both hyper- and
204 hypomethylated genes in 15 mo aSyn Tg vs. Wt mice were mostly hypomethylated and
205 involved in synaptic processes, especially at the pre-and post-synapse. However, at 3 mo,
206 most of the differentially methylated genes were hypermethylated.

207

208 **The levels of m6A regulatory proteins do not change in different brain regions in Wt and**
209 **aSyn Tg mice**

210 To validate the meRIP-Seq results and to evaluate if the overall levels of the m6A
211 modification are affected in aSyn Tg vs. Wt mice, we performed an m6A ELISA, for total RNA
212 isolated from cortical and midbrain brain tissue of young and aged, Wt and aSyn Tg mice.
213 We found that overall, the levels of m6A modification marks were higher in the cortex
214 compared to the midbrain. In cortical brain tissue, we observed that the m6A marks in the
215 aSyn Tg mice do not display the same pattern as in Wt animals (Figure 3A). A significant
216 reduction in m6A marks was observed in 12 mo aSyn Tg mice compared to 12 mo Wt mice
217 (Wt; mean = 0.032 ± 0.018 OD, aSyn Tg; mean = 0.011 ± 0.002 OD, adjusted p-value =
218 0.045). In the younger animals, however not significant, a slight reduction in m6A marks was
219 observed in 3 mo aSyn Tg were compared with 3 mo Wt mice, indicative of an effect that
220 probably starts at a young age and progresses with ageing (Figure 3A). In the midbrain, we
221 did not observe significant differences in the m6A marks between the groups (Figure 3A).
222 This is consistent with the meRIP-Seq data where we observed that the total number of
223 differentially methylated transcripts was not altered among the groups (Figure 1A, B). This
224 suggests that despite the observed hypo- and hyper-methylation in certain transcripts
225 (Figure 1D) the overall m6A levels remain in an equilibrium in the midbrain.

226 Next, we asked if the observed changes in the m6A marks in the cortex correlate with
227 altered levels of the three m6A regulatory proteins in the cortical brain tissue. To do so, we
228 performed immunoblotting analysis to assess the expression of m6A regulators — METTL3,
229 YTHDF1, and FTO. We used three different age groups – 3 mo, 6mo and 12 mo from the Wt
230 and aSyn Tg mice for our analysis. We observed no significant differences in the expression

231 levels of these m6A regulatory proteins neither within genotypes (Tg vs. Wt) nor across the
232 different age groups (Figure 3B). Nonetheless, we observed a trend towards a reduction in
233 the levels of METTL3 and FTO in Wt mice during ageing (Figure 3B).

234 Considering no difference in the protein levels of m6A regulators, we sought to identify if
235 the sub-regional and/or subcellular localisation of the three m6A regulatory proteins is
236 altered. For this, we assessed the levels of METTL3, YTHDF1 and FTO by
237 immunofluorescence intensity analysis in four different regions of the mouse brain, namely
238 cortex, striatum, hippocampus, and cerebellum. MAP2 co-staining was used only to identify
239 the neurons present in the areas of the brain. All these proteins were present in our
240 selected areas of interest, but their compartmentalization varied across different regions of
241 the neurons.

242 The m6A writer protein, METTL3 was observed as small puncta within the nucleus in the
243 cortex, striatum, hippocampus, and cerebellum in both aged Wt and aSyn Tg brain (Figure
244 4A). We found no significant differences in protein levels between aSyn Tg vs. Wt mice
245 based on the fluorescence intensity (Figure 4B).

246 The m6A reader protein, YTHDF1, on the other hand, localised only in the soma of neurons
247 in all four areas of interest, with a similar expression pattern in Wt and aSyn Tg mouse brain
248 slices. (Figure 4A). No significant difference in the fluorescence intensity of the protein was
249 observed in 15 mo aSyn Tg mice when they were compared with Wt mice (Figure 4B).

250 Finally, the m6A eraser, FTO, was detected in the nucleus and the soma of cells in the
251 cortex, striatum, hippocampus, and cerebellum. FTO was also localized in the dendrites of
252 neurons in the cortex and cerebellum in both Wt and aSyn Tg mouse brain slices (Figure 4A).

253 After analysis of the expression of this protein in the soma, no significant differences were
254 observed in the different regions of either aSyn Tg or Wt mice (Figure 4B).

255 Our findings show that the m6A regulatory proteins – METTL3, YTHDF1 and FTO are present
256 in the cortex, striatum, hippocampus, and the cerebellum in the mouse brain. In addition,
257 we found that the levels of METTL3, YTHDF1 and FTO do not change in cortical brain tissue.

258

259 **METTL3 is reduced in the aSyn Tg mouse post-synapse**

260 Based on our bioinformatics analysis, we observed that the majority of m6a genes were
261 synaptic, so we asked if/and to what degree the m6A regulators are present at synapses
262 acting as local regulators since the overall regulator levels remain unchanged. We used
263 primary cortical neurons that allow higher imaging potential and performed co-staining of
264 the three m6A regulatory proteins – METTL3, YTHDF1 and FTO alongside Syn1, pre-synaptic
265 marker and PSD95, post-synaptic marker to study the localisation of these proteins at the
266 synapse. Previous studies have indicated reduced synaptic activity in neurons derived from
267 sporadic PD patients when compared with controls [65,66].

268 Two experimenters performed the colocalisation analysis, and similar results were obtained.
269 METTL3 was observed to be present in the nucleus as nuclear speckles and it significantly
270 co-localized with PSD95, indicating its presence at the post-synapse in both Wt (PCC = 0.810
271 ± 0.039) and aSyn Tg (PCC = 0.748 ± 0.075) primary neurons. In contrast, METTL3 did not co-
272 localize with synaptotagmin1 in Wt (PCC: 0.489 ± 0.086) or aSyn Tg (PCC: 0.476 ± 0.050)
273 primary neurons, indicating no noticeable localisation at the pre-synapse (Figure 5B).

274 Similarly, we investigated the compartmentalization of YTHDF1, which did not overlap with
275 either synaptotagmin1 (PCC: Wt = 0.382 ± 0.090, aSyn Tg = 0.294 ± 0.065) or PSD95 (PCC:
276 Wt = 0.310 ± 0.088, aSyn Tg = 0.280 ± 0.069) (Figure 5B). The m6A eraser protein, FTO, was
277 identified within the cell nucleus and in some cases, in the soma of primary neurons. No
278 significant co-localisation of FTO was observed at the pre- (PCC, Wt = 0.468 ± 0.109, aSyn Tg
279 = 0.488 ± 0.095) or post-synapse (PCC, Wt = 0.366 ± 0.063, aSyn Tg = 0.463 ± 0.081) (Figure
280 5B).

281 Overall, we observed that the expression of METTL3 was reduced at the post-synapse in
282 aSyn Tg primary neurons suggesting a possible loss of METTL3 at the synapse.

283

284 **Primary neurons from aSyn Tg mice have a greater number of synapses than Wt animals**

285 Since we observed a reduction in the localisation of METTL3 at the synapse in aSyn Tg
286 primary neurons, we wondered whether this has any influence on the synapse morphology
287 and number, or vice versa. For this, we used primary cortical neurons and performed
288 proximity analysis of the pre-and post-synaptic markers Syn1 and PSD95 using the IMARIS
289 software Imaris (RRID: SCR_007370) and the data were analysed blindly to avoid bias. We
290 found that the number of synapses in aSyn Tg primary neurons was significantly increased
291 when compared with Wt neurons (Wt; mean = 2607 ± 763.1, aSyn Tg; mean = 3152 ± 1187,
292 p-value = 0.044) (Figure 6).

293

294 ## Discussion

295 The involvement of epitranscriptomics in PD is still not well understood. In this study, our
296 objective was to begin to unravel the role of m6A RNA methylation in the A30P aSyn Tg
297 mouse model of PD/synucleinopathy, in disease and physiological ageing.

298 Our findings revealed that 99.5% of the transcripts were hypermethylated in 15 mo vs. 3 mo
299 Wt mice suggesting that ageing might contribute to a significant increase in m6A
300 methylation. This observation aligns with a recent study that has demonstrated an increase
301 in m6A methylation during ageing in both mice and humans [36]. This indicates that the
302 accumulation of m6A methylation marks might be a general feature of ageing in the brain,
303 potentially influencing various biological processes. It has also been shown that these
304 epigenetic changes arise mainly in young and aged mice, while during the adolescent stage
305 these genes are stabilised [68]. In contrast, when comparing 15 mo aSyn Tg mice with their
306 3 mo counterpart littermates, more transcripts were hypomethylated. This decrease in
307 methylation with age in aSyn Tg mice might suggest that the loss of methylation might be
308 related to aSyn expression/pathology. There is a possibility that the overexpressed aSyn is
309 somehow interacting with the m6A regulators and inhibiting methylation. Previous studies
310 have shown that the 6-hydroxydopamine rat PD model has significantly reduced m6A levels
311 in the striatal brain region and in the cellular model of PD [69]. Similarly, a reduction in the
312 total levels of m6A was also reported in the MPTP-treated PD mouse model and in MPP+-
313 treated MN9D cells [70].

314 The effect of aSyn expression was more directly studied in the comparison between 3 mo
315 aSyn Tg and Wt mice. The increase in methylation suggests that aSyn expression may be

316 linked to enhanced methylation activity in early life. However, in 15 mo aSyn Tg vs. Wt mice,
317 we observed more hypomethylated genes, suggesting that A30P aSyn expression, and likely
318 pathology, might interfere with the writing or erasing of methylation marks during ageing.
319 Importantly, our results are in accordance with a recent publication suggesting that the
320 levels of m6A are significantly lower in PD patients [71].

321 Interestingly, based on GO term analysis, we found that differentially methylated transcripts
322 were predominantly associated with synaptic function and that methylation was lost with
323 ageing. Hypermethylation of transcripts involved in the synaptic processes might lead to an
324 inhibition of mRNA translation and thereafter reduced functionality of the synapse. This is
325 particularly relevant as more than half of the causative genes and risk factors in PD have
326 been identified to function at the synapse [72] and this change in methylation pattern might
327 indirectly affect the functioning of the synapse. Considering that different RNA-based
328 epigenetic mechanisms occur locally at the synapse, this underscores their potential
329 importance in synaptic regulation [74]. Additionally, GO term analysis of the differentially
330 expressed transcripts showed a strong enrichment in immune response-related pathways.
331 Notably, m6A is implicated in the regulation of inflammation under physiological and
332 pathological conditions, known as “inflammatory ageing”, or inflammaging. This is a chronic
333 inflammatory state arising during ageing and it is characterised by an increase in pro-
334 inflammatory factors such as tumor necrosis factor (TNF-α), interleukins (IL-1β and IL-6), and
335 C-reactive protein (CRP), to name just a few [73].

336 The assessment of total m6A methylation marks showed a significant reduction in the cortex
337 of 12 mo aSyn Tg mice when compared with age-matched Wt mice. This suggests that the
338 overall m6A methylation decreases in the ageing brain. This finding is consistent with recent

339 studies that reported a predominant reduction in m6A methylation in the frontal cortex and
340 cingulate cortex from PD patients [71,75]. In vitro studies have also reported a significant
341 reduction in m6A levels in the cellular PD models [70]. Despite this, we observed similar
342 expression levels of m6A regulatory proteins. However, our findings are consistent with
343 those from a recent study reporting that the levels of YTHDF1 and FTO mRNA remain
344 unchanged in PD. However, a reduction in the levels of METTL3 mRNA in PD patients was
345 also reported in that study, in contrast to what we observed [71]. Some studies have also
346 reported up-regulation of ALKBH5, IGF2BP2 in the substantia nigra while, YTHDF1 and
347 fragile X mRNA (FMR1) were downregulated. In the striatum, an up-regulation of FMR1 and
348 Cbl proto-oncogene like 1 (CBLL1) and down-regulation of METTL3, RBM15 and IGF2BP3
349 was observed [76].

350 Although we found no significant differences in the levels of m6A regulatory proteins, we
351 observed that the three proteins were present in the cortex, striatum, hippocampus, and
352 cerebellum. Our findings are consistent with those from previous studies reporting that the
353 m6A-methyltransferase complex, including METTL3, is predominantly found in the nucleus,
354 but that it can also be localised in the cytoplasm [77–79]. As methylation generally occurs
355 co-transcriptionally in the nucleus, while reading occurs largely at the cytosol, YTHDF1 is
356 primarily cytosolic [80]. FTO, on the other hand, is localised both in the nucleus and in the
357 cytosol [81]. These observations suggest that an inhibitory factor affecting their function
358 and aSyn aggregation is potentially playing a role. Previous studies have shown that aSyn
359 binds to histone proteins, which may alter the protein surface due to post-translation
360 modifications of histone tails, altering their affinity for DNA and other histones [82]. Another
361 study showed that aSyn expression increases histone-H3 lysine-9 (H3K9) methylation,

362 suggesting a possible interaction of aSyn with epigenetic writer proteins [83]. This could
363 constitute a mechanism through which aSyn affects gene methylation, ultimately affecting
364 synaptic functioning [84,85].

365 Given that most of the hypermethylated genes were synaptic, we assessed the presence of
366 these regulators at the synapse. Our findings suggest the presence of METTL3 at the post-
367 synapse, indicating that the enzyme might be locally active at the synapse. The dynamic
368 nature of m6A methylation may be localised to different regions within a cell, depending on
369 the temporal requirements of the respective genes [86,87]. In another study, m6A
370 regulatory proteins were found localised adjacent to the synapse and in the dendrites, also
371 suggesting the sub-cellular localisation of m6A methylated mRNA which might lead to
372 synaptic modifications [88,89]. Our findings revealed that the expression of METTL3 is
373 reduced at the post-synapse in aSyn Tg DIV14 neurons, suggesting a possible loss of METTL3
374 at the post-synapse. Due to this reduction at an early stage, the nucleus might be sending
375 hypermethylated transcripts to the dendrites to compensate for this loss. However, this may
376 be lost during ageing. Based on our bioinformatics analysis, we observed that methylated
377 transcripts associated with synaptic function were reduced in aSyn Tg mice with ageing. This
378 suggests that a reduction in the m6A methylation in synaptic genes may be directly linked
379 with the reduced METTL3 localisation at the synapse in aSyn Tg neurons.

380

381 **Conclusion**

382 In conclusion, our study highlights the critical role of m6A RNA methylation in the
383 progression of PD and its implications in ageing, particularly focusing on the A30P aSyn

384 mouse model. Our findings indicate that aSyn expression/pathology may influence RNA
385 methylation patterns, leading to reduced levels of m6A in mice. The differentially
386 methylated transcripts were predominantly synaptic, indicating that m6A modifications play
387 a crucial role in synapse physiology and potentially contribute to the synaptic dysfunction
388 observed in PD [90]. Although we observed no significant changes in the levels of m6A
389 regulatory proteins, the reduction in METTL3 at the synapse in aSyn Tg mice informs on the
390 importance of subcellular compartmentalization of these proteins in the regulation of RNA
391 methylation. Therefore, our research provides new insights into the epigenetic mechanisms
392 underlying PD and underscores the need for further exploration of m6A RNA methylation as
393 a potential therapeutic target for PD and other related synucleinopathies.

394

395 # Materials and methods

396 **Resource availability**

397 **Lead contact for reagent and resource sharing**

398 Further information and requests for resources and reagents should be directed to and will
399 be fulfilled by the lead contact, Tiago F. Outeiro (tiago.outeiro@med.uni-goettingen.de).

400

401 **Experimental model and subject details**

402 **Animals**

403 Five male homozygous [A30P] aSyn transgenic (aSyn Tg) mice (C57BL/6J-Tg(Th-
404 SNCA*A30P*A53T) 39Eric/J, Strain #:008239, RRID: IMSR_JAX:008239) and five wild type
405 (Wt) littermates, 3 mo, 6mo, 12 mo and 15 mo were included in this study for RNA
406 sequencing and analysis. Additional animals used for each experiment are mentioned in the
407 respective section. Animals were housed in standard cages with 12h light/12h dark cycle
408 and ad libitum access to food and water in the animal facility of the University Medical
409 Centre Göttingen (Göttingen, Germany). Animal procedures were performed in accordance
410 with the European Community (Directive 2010/63/EU); and institutional and national
411 guidelines under the Lower Saxony State Office for Consumer Protection and Food Safety
412 (LAVES) (license number 19.3213). Animals were anesthetised with carbon dioxide (CO_2) and
413 then sacrificed using cervical dislocation. For tissue processing, the brain was surgically
414 extracted from the skull and was further dissected to isolate the cortex and midbrain. The
415 tissue was snap-frozen in liquid nitrogen and preserved at -80°C until use.

416 For the preparation of brain slices, the animals were perfused with 1x phosphate buffer
417 saline (PBS) followed by 4% paraformaldehyde (PFA). The whole brain was dissected out of
418 the skull and placed overnight in 4% PFA at 4°C. The following day, the brain was washed
419 once with 1x PBS and then placed in 15% saccharose and 30% saccharose with 0.1% sodium
420 azide (NaN_3). The brains were placed at 4°C until used. Sagittal cryo-sections of 30 µm
421 thickness were cryo-sectioned using Leica CM3050 S cryostat for each mouse brain. The
422 sections were placed in 1x PBS with NaN_3 until they were used for immunohistochemistry
423 (IHC) protocol.

424

425 **Neuronal cultures**

426 Primary cortical neuronal cultures were prepared from both aSyn Tg and Wt mice as
427 previously described (Saal et al., 2015). Cells were seeded on coverslips coated with poly-L-
428 ornithine (0.1 mg/mL in borate buffer; PLO) (Sigma-Aldrich, MO, USA) or culture plates
429 (Corning, Merck, Darmstadt, Germany) for immunocytochemistry and maintained in
430 neuronal cell culture medium (Neurobasal medium, Gibco Invitrogen, CA, USA),
431 supplemented with 1% penicillin-streptomycin (PAN Biotech, Aidenbach, Germany), 0.25%
432 GlutaMAX (Gibco Invitrogen, CA, USA), and 2% B27 (B-27™ Plus Supplement (50X), Gibco,
433 #A3582801). The cells were maintained at 37°C with 5% CO_2, and one-third of the medium
434 was replaced with fresh media every 3-4 days.

435

436 **Immunocytochemistry**

437 Primary neurons were first washed with 1x PBS (PAN Biotech, Aidenbach, Germany) and
438 fixed with 4% of PFA for 20 min at room temperature (RT). Cells were first permeabilized
439 with 0.1% Triton X-100 (Sigma-Aldrich, MO, USA) for 10 min and then blocked with 1.5%
440 normal goat serum (NGS) in 1x PBS (Sigma-Aldrich, MO, USA) for 1h at RT. The cells were
441 then incubated with the primary antibodies diluted in blocking solution (FTO (mouse, Abcam
442 – ab92821, 1:1000), METTL3 (rabbit, Cell Signalling - #51104, 1:1000), YTHDF1 (rabbit,
443 Proteintech 17479-1-AP, 1:1000), MAP2 (rabbit, Proteintech – #17490-1-AP, 1:1000),
444 postsynaptic density protein 95 (PSD95) (mouse, Synaptic systems 124011, 1:1000),
445 PSD95(D74D3) (rabbit, Cell Signalling - #3409, 1:1000), synaptotagmin 1 (Syn1) (mouse,
446 Synaptic systems - #105311, 1:1000) synaptotagmin1 (rabbit, Synaptic systems – 105102/3,

447 1:1000)) overnight at 4°C, with constant shaking at a speed of 40-50 rpm. The following day,
448 cells were washed three times for 10 min each with 1x PBS (PAN Biotech, Aidenbach,
449 Germany) and then incubated with fluorescently conjugated secondary antibodies (Alexa
450 Fluor 488 donkey anti-mouse IgG – Invitrogen, Alexa Fluor 488 donkey anti-rabbit IgG -
451 Invitrogen, Alexa Fluor 555 donkey anti-mouse IgG – Invitrogen, Alexa Fluor 555 donkey
452 anti-rabbit IgG – Invitrogen, Alexa fluor 633 goat anti-chicken IgG - Invitrogen) for 2h at RT,
453 on a shaker at 40-50 rpm. Lastly, nuclei were counter-stained with DAPI (Carl Roth,
454 Karlsruhe, Germany) and mounted on glass slides (Epredia™ SuperFrostPlus™ Adhesion)
455 with mounting media (Invitrogen™ Fluoromount-G™) for microscopy.

456

457 **Immunohistochemistry**

458 The free-floating tissue was carefully transferred from PBS and $NaNH_3$ to 1x tris-buffered
459 saline (TBS) in a new 24-well plate with immunohistochemistry (IHC) grids. The tissue was
460 washed three times for 5 min each with 1x TBS to remove the remnants of NaN_3. Following
461 this, tissue antigen retrieval was performed using citrate buffer (10 mM citrate, 0.05%
462 Tween 20, pH 6.0) at 90°C for 30 min in a water bath. The tissue samples were allowed to
463 cool down until they reached RT. Tissue sections were washed thrice for 10 min each with
464 1x TBS and then incubated with 0.3% Triton X-100 for 20 min. Without washing, the tissue
465 slices were incubated directly in a blocking solution (5% BSA, and 1% NGS in 1x TBS) for 2h
466 at RT. The tissue sections were then incubated for 48h with antibodies diluted 1:200 times
467 (FTO (mouse, Abcam – ab92821, 1:1000), METTL3 (rabbit, Cell Signalling - #51104, 1:1000),
468 YTHDF1 (rabbit, Proteintech #17479-1-AP, 1:1000), MAP2 (rabbit, Proteintech – #17490-1-

469 AP, 1:1000)) at 4°C, on a shaker. The following day, tissue sections were washed thrice for
470 10 min each with 1x TBS at RT. Afterwards, the tissue sections were incubated in secondary
471 antibody (1:400 dilution) (Alexa Fluor 488 donkey anti-mouse IgG – Invitrogen, Alexa Fluor
472 488 donkey anti-rabbit IgG - Invitrogen, Alexa Fluor 555 donkey anti-mouse IgG –
473 Invitrogen, Alexa Fluor 555 donkey anti-rabbit IgG – Invitrogen, Alexa fluor 633 goat anti-
474 chicken IgG - Invitrogen) overnight at 4°C on the shaker. The following day, the tissue was
475 washed thrice for 10 min each with 1x TBS to remove the unbound secondary antibody. The
476 tissue sections were incubated for 5 min in DAPI (Carl Roth, Karlsruhe, Germany) followed
477 by a 10 min wash with 1x TBS. The tissue sections were then mounted onto glass slides
478 (Epredia™ SuperFrostPlus™ Adhesion) and left to dry in the dark at RT. 8-10µl of mounting
479 media (Invitrogen™ Fluoromount - G™) was applied as a drop onto each section on the glass
480 slide and a glass coverslip (Avantor, 631-0147, 0.16-0.19mm thickness, #1.5) was carefully
481 placed on the tissue to avoid any air bubbles.

482

483 **Western blots**

484 Cortical brain tissue was extracted from three adult mice per age group (age group 2 mo, 6
485 mo and 12 mo) from each Wt and Tg mice. The tissue from adult mice was lysed using
486 homogenisation beads (1.4 mm diameter ceramic beads, 91-PCS-CK14B, PEQLAB
487 Biotechnologie, Germany) in RIPA buffer (50 mM Tris, pH 8.0, 0.15M NaCl, 0.1% SDS, 1.0%
488 NP-40, 0.5% Na-Deoxycholate, 2 mM EDTA) supplemented with protease and phosphatase
489 inhibitors cocktail (cOmplete™, Mini Protease Inhibitor Cocktail, Roche). The
490 homogenisation was performed in Precellys 24 tissue homogenizer (Bertin Instruments) at

491 65 000 × g for 2 × 30 sec runs with a 30 sec break in between. Protein concentrations in the
492 lysates were determined by the BCA protein assay (Pierce Biotechnology, #23225) following
493 the manufacturer's protocol. The spectrophotometric recordings were performed using a
494 plate reader (Tecan, Infinite® M200 pro) at 562 nm. Volume for 20 µg of protein per sample
495 was calculated, to which Laemmli sample buffer (250 mM Tris-HCl pH 6.8, 10% SDS, 1.25%
496 Bromophenol Blue, 5% ß-mercaptoethanol, 50% glycerol) was added (1:5 dilution of
497 Laemmli: protein). The proteins were denatured for 5 min at 95°C, with 600 rpm in a
498 thermal shaker. The samples were loaded on a 12% SDS-PAGE electrophoresis gel and
499 separated at 120V for approximately 1h. The proteins were then transferred to PVDF
500 membranes (iBlot2 Transfer Stack, PVDF, Life, #IB24002X3) using iBlot2 (Invitrogen, CA,
501 USA) using the P0 protocol for 7 min. Membranes were blocked with 5% BSA (Sigma Aldrich,
502 #AG9418) in TBS (pH 8) with 0.05% Tween-20 (TBS-T) and then incubated with the
503 appropriate primary antibody (FTO (mouse, Abcam – ab92821, 1:5000), METTL3 (rabbit, Cell
504 Signalling - #51104, 1:1000), YTHDF1 (rabbit, Proteintech #17479-1-AP, 1:2500)) overnight in
505 5% BSA (Sigma-Aldrich, MO, USA) in TBS-T at 4°C. After three washes with TBS-T,
506 membranes were incubated for 2h with horseradish peroxidase (HRP) conjugated secondary
507 antibodies (Cytiva sheep anti-mouse IgG, 1:8000 dilution, Cytiva donkey anti-rabbit IgG,
508 1:8000 dilution). Following incubation, membranes were washed three times with TBS-T for
509 10 min each and developed in a chemiluminescence system (Fusion FX Vilber Lourmat,
510 Vilber, France) using chemiluminescent HRP substrate (Millipore, MA, USA). Intensities of
511 specific bands were normalised to a protein loading control.

512

513 **RNA extraction**

514 For brain tissue, TRIzol reagent (Invitrogen, CA, USA) and ceramic beads (1.4 mm diameter
515 ceramic beads, 91-PCS-CK14B, PEQLAB Biotechnologie, Germany) were added in vials with
516 frozen tissue and homogenisation was performed with the Precellys 24 tissue homogenizer
517 (Bertin Instruments) at 65 000 g for 2 x 30 sec runs with a 30 sec break in between. RNA
518 isolation was performed with TRIzol reagent according to the manufacturer's instructions.
519 Briefly, 0.5 ml of TRIzol was added to the tissue samples and incubated for 5 min before
520 homogenisation. After homogenisation, 0.1 ml of chloroform was added to each tube. The
521 tubes were shaken vigorously and incubated at RT for 2-3 min. The tubes were centrifuged
522 at 14 000g, for 10min at 4°C. The top aqueous layer was carefully transferred to a fresh
523 tube. Total RNA was then precipitated using Clean and Concentrator 5, Zymo research kit
524 (Zymo Research, #R1014). Following RNA extraction and precipitation, RNA was dissolved in
525 RNAse-free water and concentration and quality were estimated with NanoDrop 1000
526 spectrophotometer (Thermo Fisher Scientific, MA, USA) by measuring absorption at 260 nm
527 and the ratios 260/280 nm and 230/280nm respectively.

528

529 **m6A fluorescence ELISA**

530 m6A RNA methylation ELISA (m6A RNA methylation, Abcam, #ab233491) was used for the
531 detection of m6A RNA methylation in the cortical brain and midbrain tissue from 3 mo and
532 12 mo/15 mo Wt and aSyn Tg mice. For this experiment, we used cortical mouse brain
533 tissue from Wt mice each at 3 mo and 12 mo (six 3 mo and six 12 mo), and aSyn Tg mice (six
534 3 mo and five 12 mo). Midbrain tissue was used from Wt mice (three 3 mo and four 15 mo)
535 and aSyn Tg mice (five 3 mo and four 15 mo). This protocol ensures that the total m6A

536 methylation is measured in both mRNAs and small RNAs. The protocol was performed
537 according to the manufacturer's protocol. Briefly, total RNA isolated from the tissue was
538 added to bind to the assay wells. The wells were then washed to remove the unbound RNA
539 and diluted capture antibody was added to the wells. Unbound capture antibody was
540 washed out with multiple washing steps. Diluted detector antibody was then added along
541 with fluoro-enhancer. The wells were washed again and incubated with fluoro developer
542 mixture to initiate the fluorescence reaction. The fluorescence was then measured at
543 590nm using plate reader (Tecan, Infinite® M200 pro).

544

545 **MeRiP**

546 Total RNA was treated with DNase to remove any DNA remnants and further, 5-10 µg of
547 total RNA was depleted for rRNA using the RiboMinus Eukaryote Ribosomal Removal Kit
548 (Invitrogen). The large RNA fraction (>200 bp) was fragmented to a fragment size of
549 approximately 100-120 nt by RNA Fragmentation Reagent at 70°C for 5 min (#AM8740,
550 Thermo Fisher Scientific, Waltham, MA). 5% of this RNA sample was kept as inputs and the
551 rest was subjected to immunoprecipitation (IP). 300 µg of fragmented RNA was used for
552 each IP. 3 µg of anti-m6A antibody was incubated with the RNA IP buffer (0.2 M Tris-HCl pH
553 7.5, 0.5 M NaCl and 2% (vol/vol) Igepal CA-630) for 2h at 4°C with constant rotation. RNA
554 antibody mixes were then crosslinked twice with 0.15 J/cm2 of UV light (254 nm) in a UVP
555 crosslinker (Analitik Jena). Antibody-RNA conjugates were incubated with 30 µl of Protein
556 A/G beads overnight (ON) at 4˚C with rotation in 500 µl IP buffer supplemented with 200
557 units. The beads with immunoprecipitated RNA were washed with IP buffer five times, and

558 further washed with low-salt (50 mM Tris pH 7.4, 50 mM NaCl, 1mM EDTA, 1, 0.1% NP-40,
559 0.1% SDS) and high-salt (same as low-salt but with 500mM NaCl) buffers at 4˚C with rotation
560 to remove any nonspecific binding. RNA was eluted by incubating in 150 µl PKD buffer
561 (Qiagen) with 10 µl of Proteinase K (Millipore) for 1 hour at 37˚C with agitation. Eluted RNA
562 was cleaned before proceeding to library preparation.

563

564 **Library Preparation and Sequencing**

565 Samples were prepared for sequencing using the SMARTer Stranded Total RNA-Seq Kit v2 —
566 Pico Input Mammalian (Takara) according to the manufacturer's protocol. All the RNA
567 obtained from the IP samples was used for library preparation, for input samples, 2 ng was
568 used. The libraries were amplified for a total of 12 cycles for input and 16 cycles for IP
569 samples. RNA-Seq samples were prepared with the TruSeq Stranded mRNA Library Prep Kit
570 (Illumina) according to the manufacturer's instructions for which, 50 ng of rRNA-depleted
571 RNA from each of the inputs was used. Prepared libraries were sequenced in a Hiseq 2000
572 System (Illumina) for 50 cycles in single-end reads. Additional metadata is also available via
573 the GEO database (GSE275432).

574

575 **Bioinformatic Analysis of meRIP-seq and RNA-seq**

576 Raw reads were processed and demultiplexed using bcl2fastq (v2.20.2), and low-quality
577 reads were filtered out with Cutadapt v1.11.0 [43]. Filtered reads were mapped to the
578 mouse (mm10) genome using the STAR aligner v2.5.2b [44]. The resulting bam files were

579 sorted and indexed, and the unmapped reads were removed using SAMtools v1.9.0 [45].
580 Methylation sites were determined using MeTPeak v1.0.0 [46], and differential methylation
581 (hypo- and hyper-methylated regions) was assessed with ExomePeak v2.16.0 [47] using 3
582 mo samples as control and 15 mo as treatment for the first comparison and for the second
583 comparison, Wt samples were used as controls while aSyn Tg were used as treatment. An
584 adjusted P value (padj, also termed as FDR [false discovery rate]) cutoff of 0.05 and FC cutoff
585 of 1.2 or 1.5 were used as indicated in the text. Only consistently significantly, differentially
586 methylated peaks were used, unless indicated.

587 For RNA-seq analyses, read counts were obtained with subread's featureCounts v1.5.1 [48]
588 from the bam files of input samples. Differential gene expression was determined by
589 DESeq2 v3.5.12 [49] using normalised read counts and correcting for covariates detected by
590 RUVseq v1.16.1 [50]. Cutoffs of padj ≤ 0.05, FC ≥ 1.2, and BaseMean ≥ 50 were applied to
591 the results (Supplementary Figure S1A, B). Background expressed genes were determined
592 for each region as those genes with a BaseMean > 50 in the corresponding input sample.

593 For visualization, bam files of both IP and input samples were collapsed for PCR duplicates
594 using SAMtools, and IP samples were normalized to their corresponding inputs and to their
595 library size using deeptools v3.2.1 [51] bamCompare. The resulting normalized tracks were
596 visualized in the IGV Browser 2.9.2 [52].

597

598 **GO Analysis**

599 GO term enrichment analyses were performed using the App ClueGO v2.5.3 [53] in
600 Cytoscape 3.7.2 [53], with GO Term Fusion enabled to collapse terms containing very similar
601 gene lists and using a custom background corresponding to expressed genes in the
602 corresponding species as obtained from RNA-seq results of the corresponding input samples
603 of the meRIP experiments. GO term tables for biological processes, cellular components,
604 pathways, and KEGG were produced and are labelled accordingly in the figures. The
605 resulting enriched GO terms were visualized with a custom script using ggplot2 v3.3.5 [54]
606 playing the adjusted p-value (padj) for the GO term, the number of genes from the list that
607 belong to said term, and the percentage of the total genes in the GO term that are present
608 in the list. Synaptic GO enrichment analyses were performed with SynGO (v1.1,
609 syngoportal.org) [55].

610

611 **Additional Bioinformatics Packages and Tools**

612 Scripts and analysis pipelines were written in R (3.5.2) [56]. Peak annotation was performed
613 with Homer v4.10.4 [57] and Annotatr v1.8.0 [58]. Guitar plots were produced with the
614 Guitar v1.20.1 [59] R package. Volcano plots were generated with plot.ly/orca v4.9.4.1 [60]
615 (Supplementary Figure S1C). Area-proportional Venn diagrams were produced with BioVenn
616 (www.biovenn.nl), and multiple list comparisons performed with Intervene / UpSet
617 (asntech.shinyapps.io/intervene/). Mouse/human homologues were determined by their
618 annotation in NCBI's HomoloGene database using the HomoloGene (v1.4.68.19.3.27) R
619 package. Odds ratios and p values to determine significance in overlapped datasets were
620 calculated with the GeneOverlap R package v1.18.0 [61]. De novo motif analyses were

621 performed with Homer's findMotifsGenome, and motifs containing the DRACH consensus
622 sequence out of the top 10 most significant are dipcasplayed. KEGG pathway enrichment
623 was produced with KEGG Mapper (www.genome.jp/kegg/mapper/) [62]. Microscopy
624 images were pre-processed with Fiji, and quantification was automated in Cell Profiler
625 (cellprofiler.org) [63]. Graphs, heat maps, and statistical analyses were performed on
626 GraphPad Prism version 9.3.1 for Mac.

627

628 **Microscopy**

629 Images of the immunofluorescence-stained neurons (three experiments in total, with at
630 least 10 regions of interest acquired per experiment) and brain tissue were acquired using a
631 confocal microscope ZEISS LSM900. The images for the neuronal cell culture were acquired
632 as a z-stack using 63x magnification with Airyscan mode. Brain slices were imaged at 40x
633 magnification, with tiles in confocal mode.

634

635 **Statistical analysis**

636 The cell culture images for m6A regulators and their colocalisation at the synapse were
637 analysed using FIJI with the plugin JaCoP, while the synapse counting was performed using
638 IMARIS. IMARIS analysis was performed following the protocol from the Queensland Brain
639 Institute. The protein signals were further classified inside the dendritic or outside using
640 membranes based on the MAP2 signals. The signals were then divided into four groups,
641 representing PSD95 inside the neuron, PSD95 outside the neuron, Synaptotagmin1 (Syn1)

642 inside the neuron and Syn1 outside the neuron. When the signal for PSD95 inside the
643 neuron was at < 500µm from the signal for Syn1, it was considered a synapse. Colocalisation
644 of synaptic markers with m6A regulators was estimated using Pearson's correlation
645 coefficient (PCC) estimated using the JaCoP plugin in ImageJ, FIJI. All IHC images were also
646 analysed for their expression levels using FIJI software. Data analysis was performed using
647 the GraphPad software version 9 for Windows (GraphPad Software, La Jolla California
648 USA, https://www.graphpad.com). For group comparisons, one-way ANOVA with Tukey's
649 test was used, while comparisons of two groups of means were done with an unpaired
650 student's t-test. All data are expressed as mean ± SD. Differences are considered significant
651 with $p < 0.05$ (*$p < 0.05$, **<0.01, ***<0.001).

652

653 **Declarations**

654 *Ethics approval*

655 Animal procedures were performed in accordance with the European Community (Directive
656 2010/63/EU); and institutional and national guidelines under the Lower Saxony State Office
657 for Consumer Protection and Food Safety (LAVES) (license number 19.3213).

658

659 *Consent for publication*

660 All authors approved the publication of the article.

661

662 *Availability of data and materials*

663 The datasets used and/or analysed during the current study are available from the
664 corresponding author upon reasonable request. All raw data files for meRIPseq are available
665 on the GEO database (GSE275432).

666

667 *Competing interests*

668 The authors declare that they have no competing interests.

669

670 *Funding*

671 TFO and AF are supported by the Deutsche Forschungsgemeinschaft (DFG, German
672 Research Foundation) under Germany's Excellence Strategy - EXC 2067/1- 390729940), and
673 by SFB1286 (Projects B6 and B8). AF is supported by the Niedersächsisches Vorab:
674 Forschungskooperation Niedersachsen – Israel (ZN3460).

675

676 *Authors' contributions*

677 AC performed, analysed, and interpreted the data from cell cultures, ELISA, IHC, and
678 western blot, and interpreted the meRIP results. MM and VG performed experiments in
679 animals. MX interpreted the data for meRIP analysis and was a major contribution in writing
680 the manuscript. YF performed and analysed ICC data. RCH performed the meRIP and

681 subsequent data analysis. AC and TO wrote the manuscript. All authors read and approved

682 the final manuscript.

683 # Figure Legends

684 **Figure 1. m6A modification landscape in ageing and aSyn Tg mice.** (A) Bar plots
685 representing the variations in the differentially expressed genes and differentially
686 methylated genes in the midbrain from aSyn Tg mice than Wt mice when 3mo mice are
687 compared with 15mo applying equal cutoffs for FC and adjusted P value (FC > 1.2 and padj ≤
688 0.05). Left: with age, right: with aSyn (B) Bar plots representing the effects of aSyn pathology
689 on differential expression and differential methylation in 3mo and 15mo Wt vs. aSyn Tg
690 mice. (C) Overview of protocols utilized in this project. (D) Pie charts representing the
691 overview of the distribution of hypomethylated, hypermethylated and mixed transcripts as
692 an effect of aSyn pathology and ageing. (E) Venn diagram representing the number of
693 differentially methylated genes involved in young and old Wt and aSyn Tg mice. It also
694 provides a summary of the overlapping genes across different genotypes. (F) Guitar plots
695 representing the distribution of m6A methylation on mRNA and lncRNA. CDS stands for
696 coding sequence, and UTR stands for untranslated region.

697

698 **Figure 2. Gene ontology (GO) analysis for 3 mo and 15 mo Wt vs. aSyn Tg mice.** (A) GO
699 analysis for the biological processes and cellular processes in 15 mo aSyn Tg vs. Wt mice,
700 FDR = 1.5. (B) Sunburst plots representing GO analysis for the genes involved in the
701 processes at the synapse in aSyn Tg vs. Wt mice at 3 mo. Graphs created with
702 syngoportal.org. (C) Sunburst plots representing GO analysis for the genes involved in the
703 processes at the synapse in aSyn Tg vs. Wt mice aged mice at 15 mo. Graphs created with
704 syngoportal.org.

705

706 **Figure 3. Levels of m6A RNA and m6A regulators in mouse brain tissue.** (A) Bar plots
707 representing the levels of m6A modification on total RNA using ELISA from cortical and
708 midbrain regions of Wt and aSyn Tg mice. A significant reduction in the levels of m6A was
709 observed in the aged, 12 mo aSyn Tg mouse cortex when compared with 12 mo Wt mice (*,
710 ajd P value = 0.045). No significant differences were observed in the midbrain region of the
711 brain. (B) Biochemical analysis using western blot comparing the expression levels of
712 METTL3, YTHDF1 and FTO in the cortical tissue from 3 mo, 6mo and 12 mo Wt vs. aSyn Tg
713 mice. Scatter plot showing no significant difference in the expression level when comparing
714 Wt with aSyn Tg mice.

715

716 **Figure 4. Distribution of m6A regulatory proteins METTL3, YTHDF1 and FTO in the cortex,**
717 **striatum, hippocampus and cerebellum of mouse brain.** (A) Representative images of
718 mouse brain tissue slices (30µm) fixed, and stained with MAP2, METTL3, YTHDF1 and FTO.
719 The images are acquired using a confocal microscope, 40x magnification with tiles, and scale
720 bar = 50µm. White arrows point to the neurons with the protein expression. (B) Bar plots
721 showing the comparison between the mean intensity of METTL3, YTHDF1 and FTO in 15mo
722 Wt vs. aSyn Tg mice.

723

724 **Figure 5. METTL3 is localised at the post-synapse in Wt and aSyn Tg DIV14 primary**
725 **neurons.** (A) Representative images of DIV14 primary neurons, fixed and stained with
726 Histone H1, MAP2, PSD95, Synaptotagmin 1, METTL3, YTHDF1, and FTO in Wt and aSyn Tg

727 neurons. Images are acquired using airy-scan at 63x magnification, scale bar = 10µm. (B) Box
728 and whisker plot representing the colocalisation of m6A regulators in Wt and aSyn Tg D-14
729 primary neurons at the pre-and post-synapse. METTL3 colocalises with the post-synapse,
730 (Pearson's correlation coefficient, Wt = 0.810, aSyn Tg = 0.748). A significant difference (*,
731 adj p value = 0.018) was observed between METTL3 at the post-synapse in Wt neurons
732 when compared with aSyn Tg neurons. (C) Box and whisker plot representing the
733 colocalisation of m6A regulators at the pre-and post-synapse in Wt and aSyn Tg primary
734 neurons. METTL3 colocalisation is significantly reduced in aSyn Tg neurons when compared
735 with Wt at the post-synapse

736

737 **Figure 6. The number of synapses is increased in aSyn Tg primary neurons**. (A)
738 Representative immunofluorescent images of DIV14 primary neurons stained with pre-
739 (Syn1, magenta) and post-synaptic (PSD95, green) markers and MAP2 in red. Acquired at
740 63x magnification, airy scan mode. Scale bar = 10µm. (B) Scatter plot for synapse counting
741 for Wt and aSyn Tg mouse models with a significant reduction in the number of synapses (*,
742 adj p value = 0.044) in aSyn Tg primary neurons when compared with Wt.

743

744 ## Supplementary Figures

745

746 **Figure S1. Gene expression analysis in aSyn Tg and Wt mice.** (A) Principle component
747 analysis (PCA) plot of total Wt vs. aSyn Tg mice (PC1 = 40.5%, PC2 = 19.2%). (B) PCA plot of
748 aSyn Tg – 3 mo and 15 mo mice, showing a clear segregation (PC1 = 49.8%, PC2 = 23.6%). (C)
749 Volcano plot showing that the expression of most of the genes is down regulated in aSyn Tg
750 mice, due to ageing (FDR < 0.05, abs(logFC) >1), aSyn Tg 15 mo vs. 3mo.

751

752 **Figure S2. Differentially expressed gene pathways in aSyn Tg 15 mo vs. 3 mo.** GO term
753 analysis comparing the enrichment of pathways, molecular function, cellular components
754 and biological processes of differentially methylated genes. Most pathway enrichment was
755 observed in immune system and immune response linked pathways including –
756 immunoglobulin binding, phagocytic vesicle, defense response and innate and adaptive
757 immune response, FC > 1.2, FDR = 1.5.

758 # References

759 1. Allis D. No Title. Epigenetics, second edition [Internet]. 2015. Available from: chrome-
760 extension://efaidnbmnnnibpcajpcglclefindmkaj/https://www.cshlpress.com/pdf/sample/2014/epige
761 netics2/EPIFM.pdf

762 2. Goldberg AD, Allis CD, Bernstein E. Epigenetics: A Landscape Takes Shape. Cell. 2007;128:635–8.

763 3. Saletore Y, Meyer K, Korlach J, Vilfan ID, Jaffrey S, Mason CE. The birth of the Epitranscriptome:
764 deciphering the function of RNA modifications. Genome Biol [Internet]. 2012;13:175. Available from:
765 http://genomebiology.biomedcentral.com/articles/10.1186/gb-2012-13-10-175

766 4. Dominissini D, Moshitch-Moshkovitz S, Schwartz S, Salmon-Divon M, Ungar L, Osenberg S, et al.
767 Topology of the human and mouse m6A RNA methylomes revealed by m6A-seq. Nature [Internet].
768 2012;485:201–6. Available from: https://www.nature.com/articles/nature11112

769 5. Liu J, Yue Y, Han D, Wang X, Fu Y, Zhang L, et al. A METTL3–METTL14 complex mediates
770 mammalian nuclear RNA N6-adenosine methylation. Nat Chem Biol [Internet]. 2014;10:93–5.
771 Available from: https://www.nature.com/articles/nchembio.1432

772 6. Ke S, Alemu EA, Mertens C, Gantman EC, Fak JJ, Mele A, et al. A majority of m 6 A residues are in
773 the last exons, allowing the potential for 3′ UTR regulation. Genes Dev [Internet]. 2015;29:2037–53.
774 Available from: http://genesdev.cshlp.org/lookup/doi/10.1101/gad.269415.115

775 7. Liu H, Begik O, Lucas MC, Ramirez JM, Mason CE, Wiener D, et al. Accurate detection of m6A RNA
776 modifications in native RNA sequences. Nat Commun [Internet]. 2019;10:4079. Available from:
777 https://www.nature.com/articles/s41467-019-11713-9

778 8. Shi H, Wei J, He C. Where, When, and How: Context-Dependent Functions of RNA Methylation
779 Writers, Readers, and Erasers. Mol Cell [Internet]. 2019;74:640–50. Available from:
780 https://linkinghub.elsevier.com/retrieve/pii/S109727651930317X

781 9. Yang Y, Hsu PJ, Chen Y-S, Yang Y-G. Dynamic transcriptomic m6A decoration: writers, erasers,
782 readers and functions in RNA metabolism. Cell Res [Internet]. 2018;28:616–24. Available from:
783 https://www.nature.com/articles/s41422-018-0040-8

784 10. Zhao BS, Wang X, Beadell A V., Lu Z, Shi H, Kuuspalu A, et al. m6A-dependent maternal mRNA
785 clearance facilitates zebrafish maternal-to-zygotic transition. Nature [Internet]. 2017;542:475–8.
786 Available from: https://www.nature.com/articles/nature21355

787 11. Dinescu S, Ignat S, Lazar AD, Constantin C, Neagu M, Costache M. Epitranscriptomic Signatures in
788 lncRNAs and Their Possible Roles in Cancer. Genes (Basel) [Internet]. 2019;10:52. Available from:
789 https://www.mdpi.com/2073-4425/10/1/52

790 12. Licht K, Jantsch MF. Rapid and dynamic transcriptome regulation by RNA editing and RNA
791 modifications. Journal of Cell Biology [Internet]. 2016;213:15–22. Available from:
792 https://rupress.org/jcb/article/213/1/15/38525/Rapid-and-dynamic-transcriptome-regulation-by-
793 RNA

794 13. Dominissini D, Moshitch-Moshkovitz S, Salmon-Divon M, Amariglio N, Rechavi G. Transcriptome-
795 wide mapping of N6-methyladenosine by m6A-seq based on immunocapturing and massively
796 parallel sequencing. Nat Protoc [Internet]. 2013;8:176–89. Available from:
797 https://www.nature.com/articles/nprot.2012.148

798 14. Bokar JA, Shambaugh ME, Polayes D, Matera AG, Rottman FM. Purification and cDNA cloning of
799 the AdoMet-binding subunit of the human mRNA (N6-adenosine)-methyltransferase. RNA [Internet].
800 1997;3:1233–47. Available from: http://www.ncbi.nlm.nih.gov/pubmed/9409616

801 15. Schwartz S, Mumbach MR, Jovanovic M, Wang T, Maciag K, Bushkin GG, et al. Perturbation of
802 m6A Writers Reveals Two Distinct Classes of mRNA Methylation at Internal and 5 Sites. Cell Rep
803 [Internet]. 2014;8:284–96. Available from:
804 https://linkinghub.elsevier.com/retrieve/pii/S2211124714004422

805 16. Pendleton KE, Chen B, Liu K, Hunter O V., Xie Y, Tu BP, et al. The U6 snRNA m 6 A
806 Methyltransferase METTL16 Regulates SAM Synthetase Intron Retention. Cell [Internet].
807 2017;169:824-835.e14. Available from:
808 https://linkinghub.elsevier.com/retrieve/pii/S0092867417305305

809 17. Patil DP, Chen C-K, Pickering BF, Chow A, Jackson C, Guttman M, et al. m6A RNA methylation
810 promotes XIST-mediated transcriptional repression. Nature [Internet]. 2016;537:369–73. Available
811 from: https://www.nature.com/articles/nature19342

812 18. Wen J, Lv R, Ma H, Shen H, He C, Wang J, et al. Zc3h13 Regulates Nuclear RNA m6A Methylation
813 and Mouse Embryonic Stem Cell Self-Renewal. Mol Cell [Internet]. 2018;69:1028-1038.e6. Available
814 from: https://linkinghub.elsevier.com/retrieve/pii/S1097276518301345

815 19. Agarwala SD, Blitzblau HG, Hochwagen A, Fink GR. RNA Methylation by the MIS Complex
816 Regulates a Cell Fate Decision in Yeast. PLoS Genet. 2012;8:e1002732.

817 20. Li Q, Li X, Tang H, Jiang B, Dou Y, Gorospe M, et al. NSUN2-Mediated m5C Methylation and
818 METTL3/METTL14-Mediated m6A Methylation Cooperatively Enhance p21 Translation. J Cell
819 Biochem [Internet]. 2017;118:2587–98. Available from:
820 https://onlinelibrary.wiley.com/doi/10.1002/jcb.25957

821 21. Xu K, Yang Y, Feng G-H, Sun B-F, Chen J-Q, Li Y-F, et al. Mettl3-mediated m6A regulates
822 spermatogonial differentiation and meiosis initiation. Cell Res [Internet]. 2017;27:1100–14. Available
823 from: https://www.nature.com/articles/cr2017100

824 22. Aguilo F, Zhang F, Sancho A, Fidalgo M, Di Cecilia S, Vashisht A, et al. Coordination of m 6 A
825 mRNA Methylation and Gene Transcription by ZFP217 Regulates Pluripotency and Reprogramming.
826 Cell Stem Cell [Internet]. 2015;17:689–704. Available from:
827 https://linkinghub.elsevier.com/retrieve/pii/S1934590915004129

828 23. Hess ME, Hess S, Meyer KD, Verhagen LAW, Koch L, Brönneke HS, et al. The fat mass and obesity
829 associated gene (Fto) regulates activity of the dopaminergic midbrain circuitry. Nat Neurosci.
830 2013;16:1042–8.

831 24. Ping X-L, Sun B-F, Wang L, Xiao W, Yang X, Wang W-J, et al. Mammalian WTAP is a regulatory
832 subunit of the RNA N6-methyladenosine methyltransferase. Cell Res [Internet]. 2014;24:177–89.
833 Available from: https://www.nature.com/articles/cr20143

834 25. Wang X, Lu Z, Gomez A, Hon GC, Yue Y, Han D, et al. N6-methyladenosine-dependent regulation
835 of messenger RNA stability. Nature [Internet]. 2014;505:117–20. Available from:
836 https://www.nature.com/articles/nature12730

837 26. Śledź P, Jinek M. Structural insights into the molecular mechanism of the m6A writer complex.
838 Elife [Internet]. 2016;5. Available from: https://elifesciences.org/articles/18434

839 27. Wang X, Feng J, Xue Y, Guan Z, Zhang D, Liu Z, et al. Structural basis of N6-adenosine methylation
840 by the METTL3–METTL14 complex. Nature. 2016;534:575–8.

841 28. Moindrot B, Cerase A, Coker H, Masui O, Grijzenhout A, Pintacuda G, et al. A Pooled shRNA
842 Screen Identifies Rbm15, Spen, and Wtap as Factors Required for Xist RNA-Mediated Silencing. Cell
843 Rep [Internet]. 2015;12:562–72. Available from:
844 https://linkinghub.elsevier.com/retrieve/pii/S2211124715006798

845 29. Jia G, Fu Y, Zhao X, Dai Q, Zheng G, Yang Y, et al. N6-Methyladenosine in nuclear RNA is a major
846 substrate of the obesity-associated FTO. Nat Chem Biol [Internet]. 2011;7:885–7. Available from:
847 https://www.nature.com/articles/nchembio.687

848 30. Zheng G, Dahl JA, Niu Y, Fedorcsak P, Huang C-M, Li CJ, et al. ALKBH5 Is a Mammalian RNA
849 Demethylase that Impacts RNA Metabolism and Mouse Fertility. Mol Cell [Internet]. 2013;49:18–29.
850 Available from: https://linkinghub.elsevier.com/retrieve/pii/S1097276512008921

851 31. Fu Y, Jia G, Pang X, Wang RN, Wang X, Li CJ, et al. FTO-mediated formation of N6-
852 hydroxymethyladenosine and N6-formyladenosine in mammalian RNA. Nat Commun [Internet].
853 2013;4:1798. Available from: https://www.nature.com/articles/ncomms2822

854 32. Alarcón CR, Lee H, Goodarzi H, Halberg N, Tavazoie SF. N6-methyladenosine marks primary
855 microRNAs for processing. Nature [Internet]. 2015;519:482–5. Available from:
856 https://www.nature.com/articles/nature14281

857 33. Zaccara S, Jaffrey SR. A Unified Model for the Function of YTHDF Proteins in Regulating m6A-
858 Modified mRNA. Cell [Internet]. 2020;181:1582-1595.e18. Available from:
859 https://linkinghub.elsevier.com/retrieve/pii/S0092867420305742

860 34. Chen J, Wei X, Yi X, Jiang D-S. RNA Modification by m6A Methylation in Cardiovascular Disease.
861 Ghose J, editor. Oxid Med Cell Longev [Internet]. 2021;2021:1–13. Available from:
862 https://www.hindawi.com/journals/omcl/2021/8813909/

863 35. Jiang Z, Wang Y, Li Z, Dai Z, He Y, Chu K, et al. The m6A mRNA demethylase FTO in granulosa cells
864 retards FOS-dependent ovarian aging. Cell Death Dis [Internet]. 2021;12:744. Available from:
865 https://www.nature.com/articles/s41419-021-04016-9

866 36. Shafik AM, Zhang F, Guo Z, Dai Q, Pajdzik K, Li Y, et al. N6-methyladenosine dynamics in
867 neurodevelopment and aging, and its potential role in Alzheimer's disease. Genome Biol.
868 2021;22:17.

869 37. Castro-Hernández R, Berulava T, Metelova M, Epple R, Peña Centeno T, Richter J, et al.
870 Conserved reduction of m ^{6} A RNA modifications during aging and neurodegeneration is linked to
871 changes in synaptic transcripts. Proceedings of the National Academy of Sciences. 2023;120.

872 38. Chen YG, Chen R, Ahmad S, Verma R, Kasturi SP, Amaya L, et al. N6-Methyladenosine
873 Modification Controls Circular RNA Immunity. Mol Cell [Internet]. 2019;76:96-109.e9. Available
874 from: https://linkinghub.elsevier.com/retrieve/pii/S1097276519305465

875 39. Yu Z, Huang L, Xia Y, Cheng S, Yang C, Chen C, et al. Analysis of m6A modification regulators in
876 the substantia nigra and striatum of MPTP-induced Parkinson's disease mice. Neurosci Lett
877 [Internet]. 2022;791:136907. Available from:
878 https://linkinghub.elsevier.com/retrieve/pii/S0304394022004682

879 40. Schapira AHV, Cooper JM, Dexter D, Jenner P, Clark JB, Marsden CD. MITOCHONDRIAL COMPLEX
880 I DEFICIENCY IN PARKINSON'S DISEASE. The Lancet [Internet]. 1989;333:1269. Available from:
881 https://linkinghub.elsevier.com/retrieve/pii/S0140673689923660

882 41. Krishnan KJ, Reeve AK, Samuels DC, Chinnery PF, Blackwood JK, Taylor RW, et al. What causes
883 mitochondrial DNA deletions in human cells? Nat Genet [Internet]. 2008;40:275–9. Available from:
884 https://www.nature.com/articles/ng.f.94

885 42. Pickrell AM, Pinto M, Hida A, Moraes CT. Striatal Dysfunctions Associated with Mitochondrial
886 DNA Damage in Dopaminergic Neurons in a Mouse Model of Parkinson's Disease. The Journal of
887 Neuroscience [Internet]. 2011;31:17649–58. Available from:
888 https://www.jneurosci.org/lookup/doi/10.1523/JNEUROSCI.4871-11.2011

889 43. Martin M. Cutadapt removes adapter sequences from high-throughput sequencing reads.
890 EMBnet J [Internet]. 2011;17:10. Available from:
891 http://journal.embnet.org/index.php/embnetjournal/article/view/200

892 44. Dobin A, Davis CA, Schlesinger F, Drenkow J, Zaleski C, Jha S, et al. STAR: ultrafast universal RNA-
893 seq aligner. Bioinformatics [Internet]. 2013;29:15–21. Available from:
894 https://academic.oup.com/bioinformatics/article/29/1/15/272537

895 45. Li H, Handsaker B, Wysoker A, Fennell T, Ruan J, Homer N, et al. The Sequence Alignment/Map
896 format and SAMtools. Bioinformatics [Internet]. 2009;25:2078–9. Available from:
897 https://academic.oup.com/bioinformatics/article/25/16/2078/204688

898 46. Cui X, Meng J, Zhang S, Chen Y, Huang Y. A novel algorithm for calling mRNA m 6 A peaks by
899 modeling biological variances in MeRIP-seq data. Bioinformatics [Internet]. 2016;32:i378–85.
900 Available from: https://academic.oup.com/bioinformatics/article/32/12/i378/2289056

901 47. Meng J, Cui X, Rao MK, Chen Y, Huang Y. Exome-based analysis for RNA epigenome sequencing
902 data. Bioinformatics [Internet]. 2013;29:1565–7. Available from:
903 https://academic.oup.com/bioinformatics/article/29/12/1565/291595

904 48. Liao Y, Smyth GK, Shi W. The Subread aligner: fast, accurate and scalable read mapping by seed-
905 and-vote. Nucleic Acids Res [Internet]. 2013;41:e108–e108. Available from:
906 https://academic.oup.com/nar/article/41/10/e108/1075719

907 49. Love MI, Huber W, Anders S. Moderated estimation of fold change and dispersion for RNA-seq
908 data with DESeq2. Genome Biol [Internet]. 2014;15:550. Available from:
909 http://genomebiology.biomedcentral.com/articles/10.1186/s13059-014-0550-8

910 50. Risso D, Ngai J, Speed TP, Dudoit S. Normalization of RNA-seq data using factor analysis of
911 control genes or samples. Nat Biotechnol [Internet]. 2014;32:896–902. Available from:
912 https://www.nature.com/articles/nbt.2931

913 51. Ramírez F, Ryan DP, Grüning B, Bhardwaj V, Kilpert F, Richter AS, et al. deepTools2: a next
914 generation web server for deep-sequencing data analysis. Nucleic Acids Res [Internet].
915 2016;44:W160–5. Available from: https://academic.oup.com/nar/article-
916 lookup/doi/10.1093/nar/gkw257

917 52. Robinson JT, Thorvaldsdóttir H, Winckler W, Guttman M, Lander ES, Getz G, et al. Integrative
918 genomics viewer. Nat Biotechnol [Internet]. 2011;29:24–6. Available from:
919 https://www.nature.com/articles/nbt.1754

920 53. Bindea G, Mlecnik B, Hackl H, Charoentong P, Tosolini M, Kirilovsky A, et al. ClueGO: a Cytoscape
921 plug-in to decipher functionally grouped gene ontology and pathway annotation networks.
922 Bioinformatics. 2009;25:1091–3.

923 54. Shannon P, Markiel A, Ozier O, Baliga NS, Wang JT, Ramage D, et al. Cytoscape: A Software
924 Environment for Integrated Models of Biomolecular Interaction Networks. Genome Res [Internet].
925 2003;13:2498–504. Available from: http://genome.cshlp.org/lookup/doi/10.1101/gr.1239303

926 55. Wickham H. Toolbox. ggplot2. New York, NY: Springer New York; 2009. p. 65–90.

927 56. Koopmans F, van Nierop P, Andres-Alonso M, Byrnes A, Cijsouw T, Coba MP, et al. SynGO: An
928 Evidence-Based, Expert-Curated Knowledge Base for the Synapse. Neuron. 2019;103:217-234.e4.

929 57. R Development Core Team. R: A Language and Environment for Statistical Computing. R
930 Foundation for Statistical Computing [Internet]. 2015. Available from: http://www.r-project.org

931 58. Heinz S, Benner C, Spann N, Bertolino E, Lin YC, Laslo P, et al. Simple Combinations of Lineage-
932 Determining Transcription Factors Prime cis-Regulatory Elements Required for Macrophage and B
933 Cell Identities. Mol Cell [Internet]. 2010;38:576–89. Available from:
934 https://linkinghub.elsevier.com/retrieve/pii/S1097276510003667

935 59. Cavalcante RG, Sartor MA. annotatr: genomic regions in context. Valencia A, editor.
936 Bioinformatics [Internet]. 2017;33:2381–3. Available from:
937 https://academic.oup.com/bioinformatics/article/33/15/2381/3092365

938 60. Cui X, Wei Z, Zhang L, Liu H, Sun L, Zhang S-W, et al. Guitar: An R/Bioconductor Package for Gene
939 Annotation Guided Transcriptomic Analysis of RNA-Related Genomic Features. Biomed Res Int
940 [Internet]. 2016;2016:1–8. Available from: http://www.hindawi.com/journals/bmri/2016/8367534/

941 61. Sievert C. Interactive Web-Based Data Visualization with R, plotly, and shiny. Chapman and
942 Hall/CRC; 2020.

943 62. L Shen. C. Sievert, Interactive Web-Based Data Visualization with R, Plotly, and Shiny (Champ
944 Hall, 2019). 2014.

945 63. Kanehisa M, Sato Y, Kawashima M. <scp>KEGG</scp> mapping tools for uncovering hidden
946 features in biological data. Protein Science. 2022;31:47–53.

947 64. Jones TR, Kang IH, Wheeler DB, Lindquist RA, Papallo A, Sabatini DM, et al. CellProfiler Analyst:
948 data exploration and analysis software for complex image-based screens. BMC Bioinformatics
949 [Internet]. 2008;9:482. Available from:
950 https://bmcbioinformatics.biomedcentral.com/articles/10.1186/1471-2105-9-482

951 65. Xylaki M, Paiva I, Al-Azzani M, Gerhardt E, Jain G, Islam MR, et al. miR-101a-3p Impairs Synaptic
952 Plasticity and Contributes to Synucleinopathy. J Parkinsons Dis. 2023;13:179–96.

953 66. Koopmans F, van Nierop P, Andres-Alonso M, Byrnes A, Cijsouw T, Coba MP, et al. SynGO: An
954 Evidence-Based, Expert-Curated Knowledge Base for the Synapse. Neuron. 2019;103:217-234.e4.

955 67. Stern S, Lau S, Manole A, Rosh I, Percia MM, Ben Ezer R, et al. Reduced synaptic activity and
956 dysregulated extracellular matrix pathways in midbrain neurons from Parkinson's disease patients.
957 NPJ Parkinsons Dis. 2022;8:103.

958 68. Rosh I, Tripathi U, Hussein Y, Rike WA, Djamus J, Shklyar B, et al. Synaptic dysfunction and
959 extracellular matrix dysregulation in dopaminergic neurons from sporadic and E326K-GBA1
960 Parkinson's disease patients. NPJ Parkinsons Dis. 2024;10:38.

961 69. Licatalosi DD, Mele A, Fak JJ, Ule J, Kayikci M, Chi SW, et al. HITS-CLIP yields genome-wide
962 insights into brain alternative RNA processing. Nature. 2008;456:464–9.

963 70. Chen X, Yu C, Guo M, Zheng X, Ali S, Huang H, et al. Down-Regulation of m6A mRNA Methylation
964 Is Involved in Dopaminergic Neuronal Death. ACS Chem Neurosci. 2019;10:2355–63.

965 71. Geng Y, Long X, Zhang Y, Wang Y, You G, Guo W, et al. FTO-targeted siRNA delivery by MSC-
966 derived exosomes synergistically alleviates dopaminergic neuronal death in Parkinson's disease via
967 m6A-dependent regulation of ATM mRNA. J Transl Med. 2023;21:652.

968 72. He H, Zhang Q, Liao J, Lei J, Luo M, Huang J, et al. <scp>METTL14</scp> is decreased and
969 regulates <scp> m ^{6} A </scp> modification of α-synuclein in Parkinson's disease. J Neurochem.
970 2023;166:609–22.

971 73. Soukup S, Vanhauwaert R, Verstreken P. Parkinson's disease: convergence on synaptic
972 homeostasis. EMBO J. 2018;37.

973 74. Liu-Yesucevitz L, Bassell GJ, Gitler AD, Hart AC, Klann E, Richter JD, et al. Local RNA Translation at
974 the Synapse and in Disease: Figure 1. The Journal of Neuroscience. 2011;31:16086–93.

975 75. Sun J, Cheng B, Su Y, Li M, Ma S, Zhang Y, et al. The Potential Role of m6A RNA Methylation in the
976 Aging Process and Aging-Associated Diseases. Front Genet. 2022;13.

977 76. Martinez De La Cruz B, Gell C, Markus R, Macdonald I, Fray R, Knight HM. m ^{6} A mRNA
978 methylation in human brain is disrupted in Lewy body disorders. Neuropathol Appl Neurobiol.
979 2023;49.

980 77. Yu Z, Huang L, Xia Y, Cheng S, Yang C, Chen C, et al. Analysis of m6A modification regulators in
981 the substantia nigra and striatum of MPTP-induced Parkinson's disease mice. Neurosci Lett.
982 2022;791:136907.

983 78. Harper JE, Miceli SM, Roberts RJ, Manley JL. Sequence specificity of the human mRNA N6-
984 adenosine methylase *in vitro*. Nucleic Acids Res. 1990;18:5735–41.

985 79. Bokar JA, Shambaugh ME, Polayes D, Matera AG, Rottman FM. Purification and cDNA cloning of
986 the AdoMet-binding subunit of the human mRNA (N6-adenosine)-methyltransferase. RNA.
987 1997;3:1233–47.

988 80. Ping X-L, Sun B-F, Wang L, Xiao W, Yang X, Wang W-J, et al. Mammalian WTAP is a regulatory
989 subunit of the RNA N6-methyladenosine methyltransferase. Cell Res. 2014;24:177–89.

990 81. Zou Z, Sepich-Poore C, Zhou X, Wei J, He C. The mechanism underlying redundant functions of
991 the YTHDF proteins. Genome Biol. 2023;24:17.

992 82. Gulati P, Avezov E, Ma M, Antrobus R, Lehner P, O'Rahilly S, et al. Fat mass and obesity-related
993 (FTO) shuttles between the nucleus and cytoplasm. Biosci Rep. 2014;34.

994 83. Goers J, Manning-Bog AB, McCormack AL, Millett IS, Doniach S, Di Monte DA, et al. Nuclear
995 Localization of α-Synuclein and Its Interaction with Histones. Biochemistry. 2003;42:8465–71.

996 84. Sugeno N, Jäckel S, Voigt A, Wassouf Z, Schulze-Hentrich J, Kahle PJ. α-Synuclein enhances
997 histone H3 lysine-9 dimethylation and H3K9me2-dependent transcriptional responses. Sci Rep.
998 2016;6:36328.

999 85. Surguchov A. α-Synuclein and Mechanisms of Epigenetic Regulation. Brain Sci. 2023;13:150.

1000 86. Jowaed A, Schmitt I, Kaut O, Wüllner U. Methylation Regulates Alpha-Synuclein Expression and Is
1001 Decreased in Parkinson's Disease Patients' Brains. The Journal of Neuroscience. 2010;30:6355–9.

1002 87. Merkurjev D, Hong W-T, Iida K, Oomoto I, Goldie BJ, Yamaguti H, et al. Synaptic N6-
1003 methyladenosine (m6A) epitranscriptome reveals functional partitioning of localized transcripts. Nat
1004 Neurosci. 2018;21:1004–14.

1005 88. Flamand MN, Meyer KD. The epitranscriptome and synaptic plasticity. Curr Opin Neurobiol.
1006 2019;59:41–8.

1007 89. Madugalle SU, Meyer K, Wang DO, Bredy TW. RNA N6-Methyladenosine and the Regulation of
1008 RNA Localization and Function in the Brain. Trends Neurosci. 2020;43:1011–23.

1009 90. Flamand MN, Meyer KD. m6A and YTHDF proteins contribute to the localization of select
1010 neuronal mRNAs. Nucleic Acids Res. 2022;50:4464–83.

1011 91. Picconi B, Piccoli G, Calabresi P. Synaptic Dysfunction in Parkinson's Disease. 2012. p. 553–72.

1012

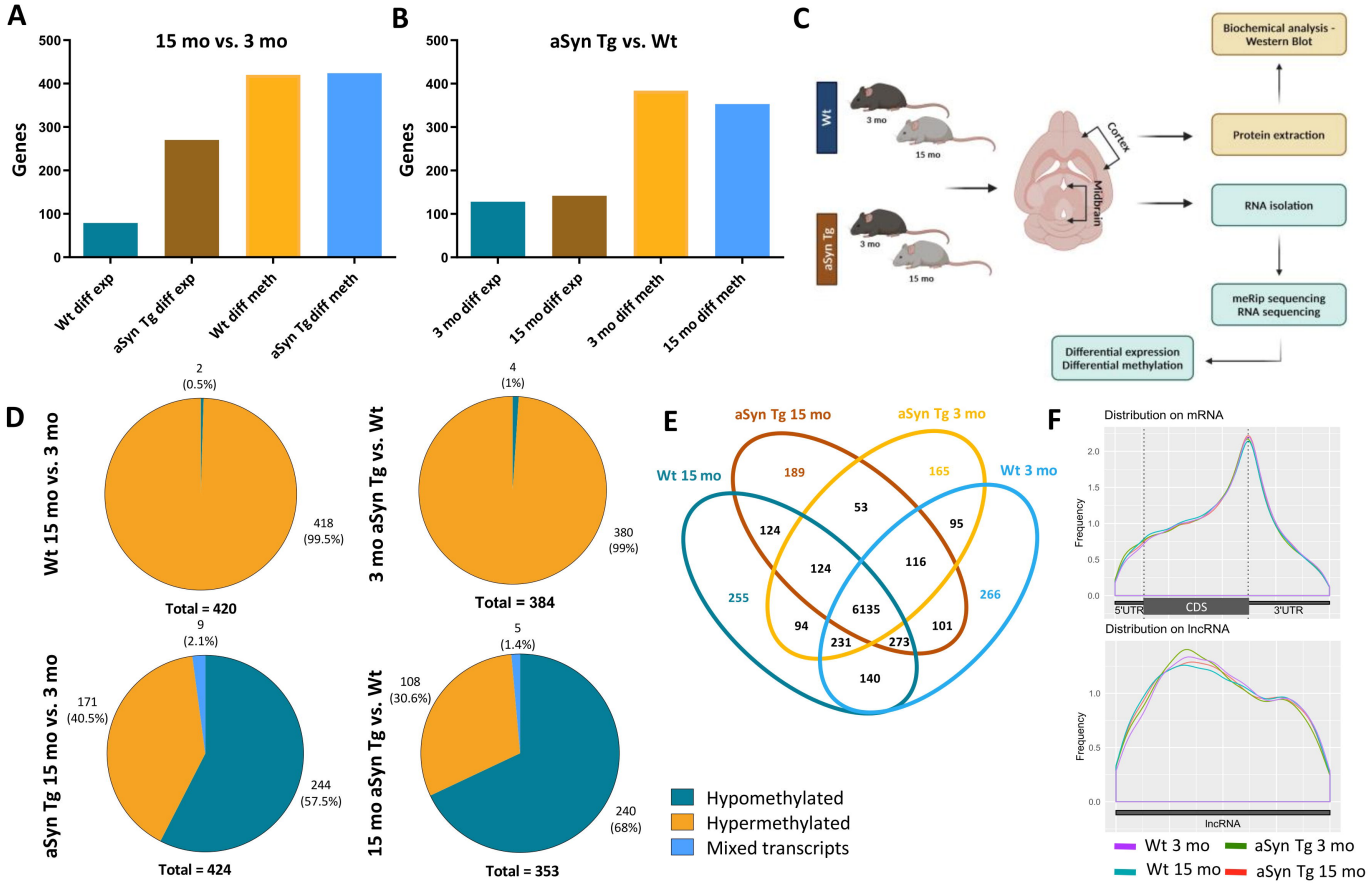
A
15 mo vs. 3 mo
Genes
500
400
300
200
100
0
Wt diff exp
aSyn Tg diff exp
Wt diff meth
aSyn Tg diff meth
B
aSyn Tg vs. Wt
Genes
3 mo diff exp
15 mo diff exp
3 mo diff meth
15 mo diff meth
C
Wt
aSyn Tg
3 mo
15 mo
Cortex
Midbrain
Biochemical analysis - Western Blot
Protein extraction
RNA isolation
meRip sequencing
RNA sequencing
Differential expression
Differential methylation
D
Wt 15 mo vs. 3 mo
2 (0.5%)
418 (99.5%)
Total = 420
3 mo aSyn Tg vs. Wt
4 (1%)
380 (99%)
Total = 384
aSyn Tg 15 mo vs. 3 mo
9 (2.1%)
171 (40.5%)
244 (57.5%)
Total = 424
15 mo aSyn Tg vs. Wt
5 (1.4%)
108 (30.6%)
240 (68%)
Total = 353
E
aSyn Tg 15 mo
aSyn Tg 3 mo
Wt 15 mo
Wt 3 mo
189
165
53
124
95
124
116
255
266
6135
94
101
231
273
140
Hypomethylated
Hypermethylated
Mixed transcripts
F
Distribution on mRNA
Frequency
5'UTR
CDS
3'UTR
Distribution on lncRNA
lncRNA
Wt 3 mo
aSyn Tg 3 mo
Wt 15 mo
aSyn Tg 15 mo

Figure 1.

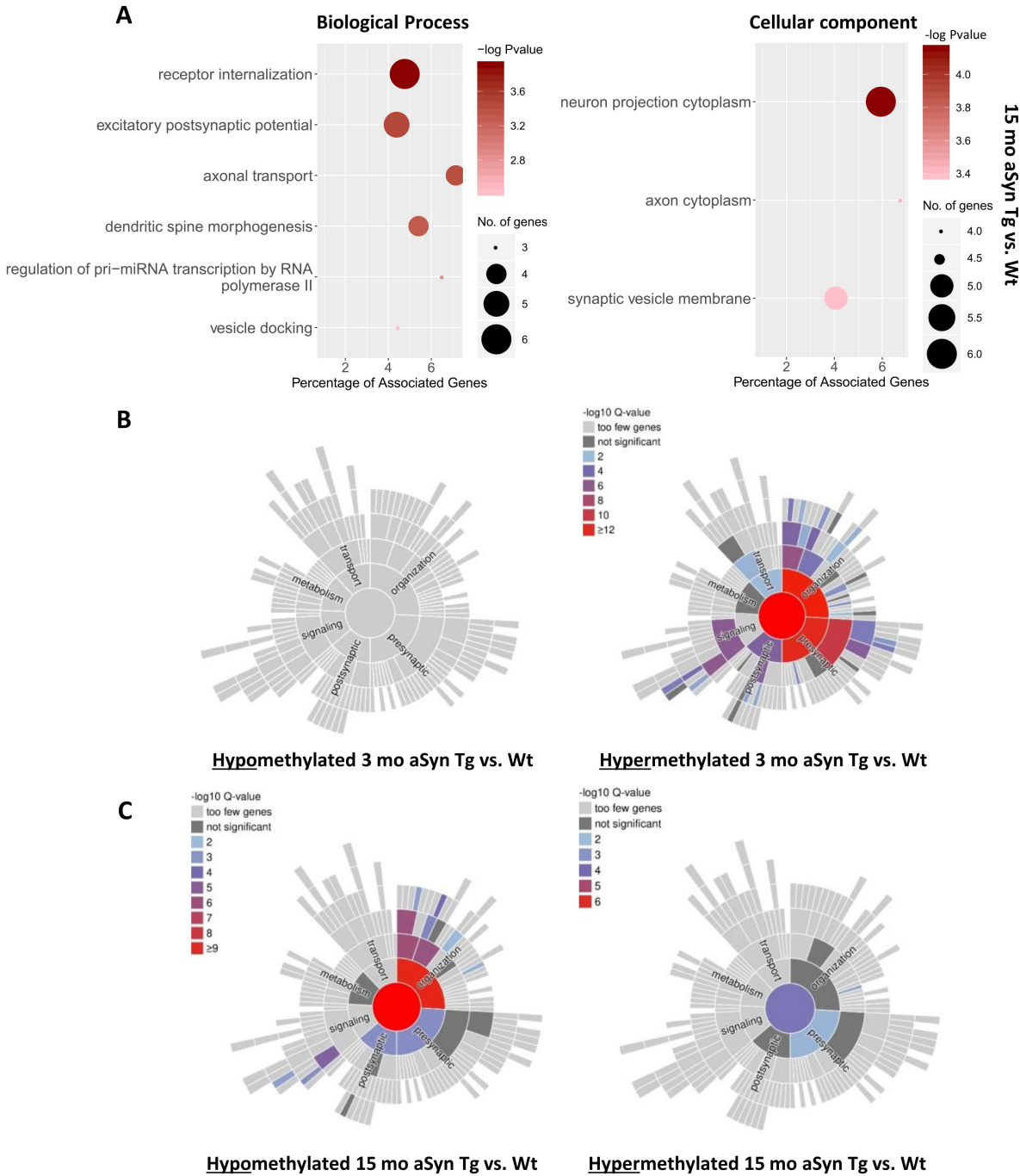
A
Biological Process
receptor internalization
excitatory postsynaptic potential
axonal transport
dendritic spine morphogenesis
regulation of pri−miRNA transcription by RNA polymerase II
vesicle docking
−log Pvalue
3.6
3.2
2.8
No. of genes
3
4
5
6
2
4
6
Percentage of Associated Genes
Cellular component
neuron projection cytoplasm
axon cytoplasm
synaptic vesicle membrane
-log Pvalue
4.0
3.8
3.6
3.4
No. of genes
4.0
4.5
5.0
5.5
6.0
2
4
6
Percentage of Associated Genes
15 mo aSyn Tg vs. Wt
B
-log10 Q-value
too few genes
not significant
2
4
6
8
10
≥12
transport
organization
metabolism
signaling
postsynaptic
presynaptic
Hypomethylated 3 mo aSyn Tg vs. Wt
Hypermethylated 3 mo aSyn Tg vs. Wt
C
-log10 Q-value
too few genes
not significant
2
3
4
5
6
7
8
≥9
transport
organization
metabolism
signaling
postsynaptic
presynaptic
Hypomethylated 15 mo aSyn Tg vs. Wt
Hypermethylated 15 mo aSyn Tg vs. Wt

Figure 2.

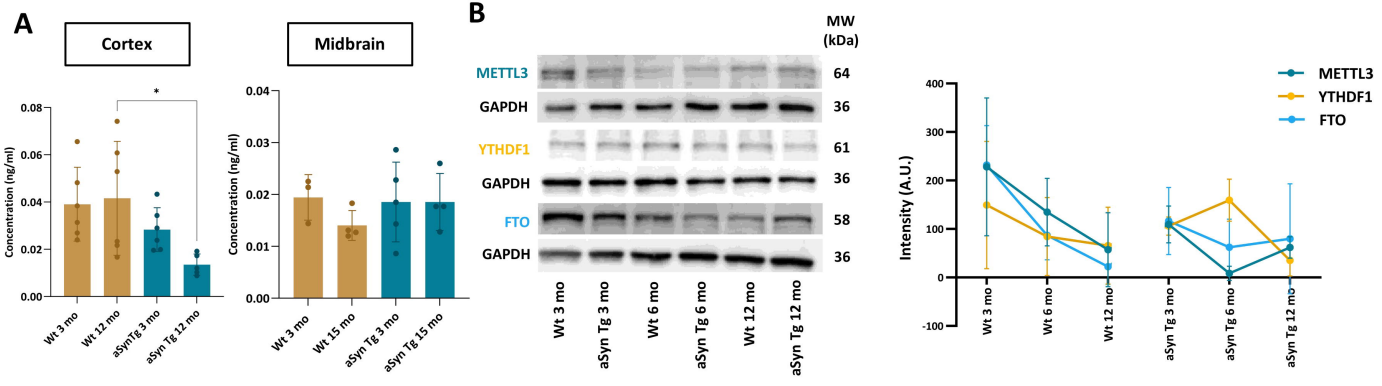
A
Cortex
Midbrain
*
Concentration (ng/ml)
0.08
0.06
0.04
0.02
0.00
0.03
0.02
0.01
Wt 3 mo
Wt 12 mo
aSynTg 3 mo
aSyn Tg 12 mo
Wt 15 mo
aSyn Tg 3 mo
aSyn Tg 15 mo
B
MW (kDa)
METTL3
GAPDH
YTHDF1
FTO
64
36
61
58
Wt 3 mo
aSyn Tg 3 mo
Wt 6 mo
aSyn Tg 6 mo
Wt 12 mo
aSyn Tg 12 mo
METTL3
YTHDF1
FTO
Intensity (A.U.)
400
300
200
100
0
-100

Figure 3.

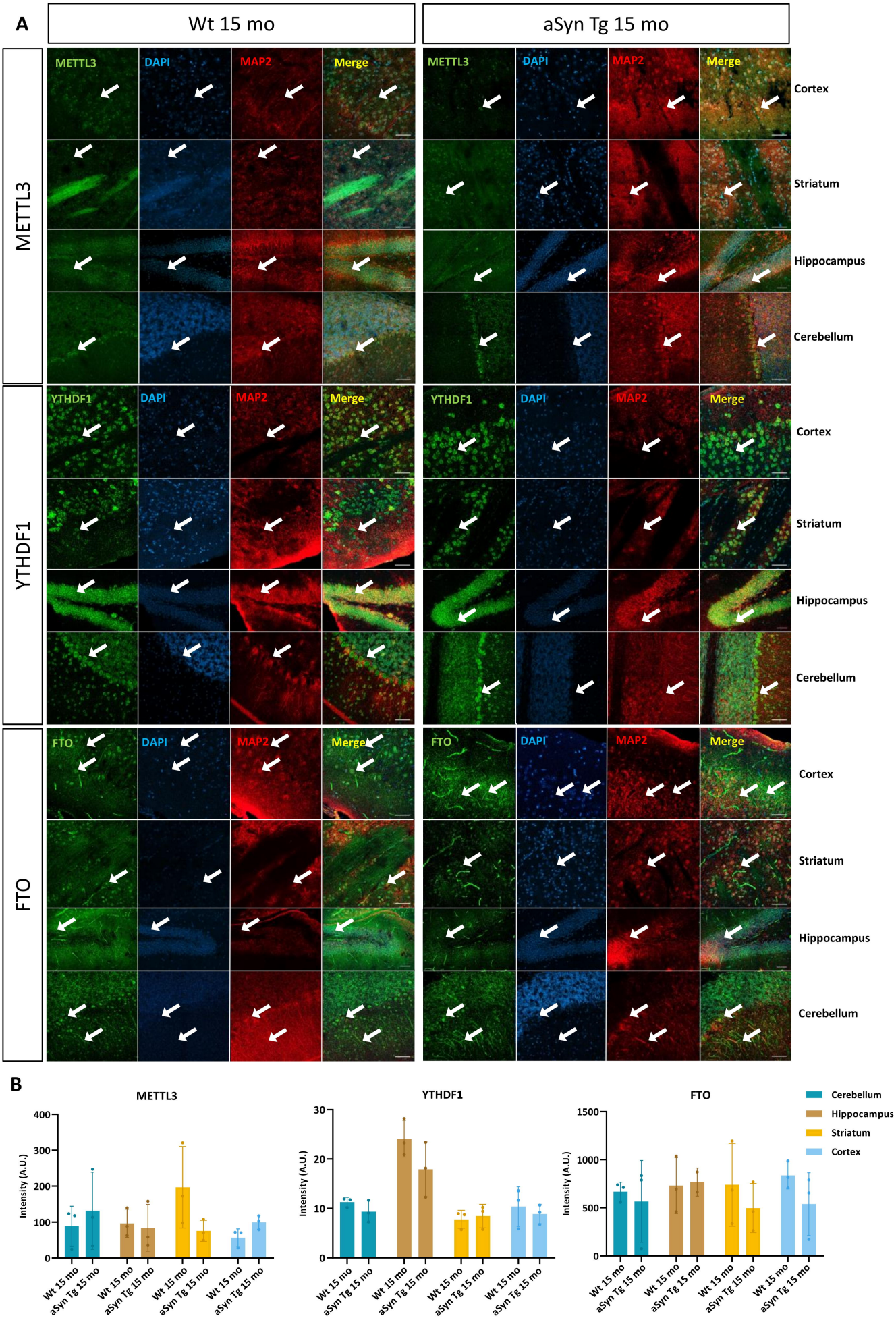
A
Wt 15 mo
aSyn Tg 15 mo
METTL3
YTHDF1
FTO
METTL3
DAPI
MAP2
Merge
Cortex
Striatum
Hippocampus
Cerebellum
B
METTL3
YTHDF1
FTO
Intensity (A.U.)
Wt 15 mo
aSyn Tg 15 mo
Cerebellum
Hippocampus
Striatum
Cortex

Figure 4.

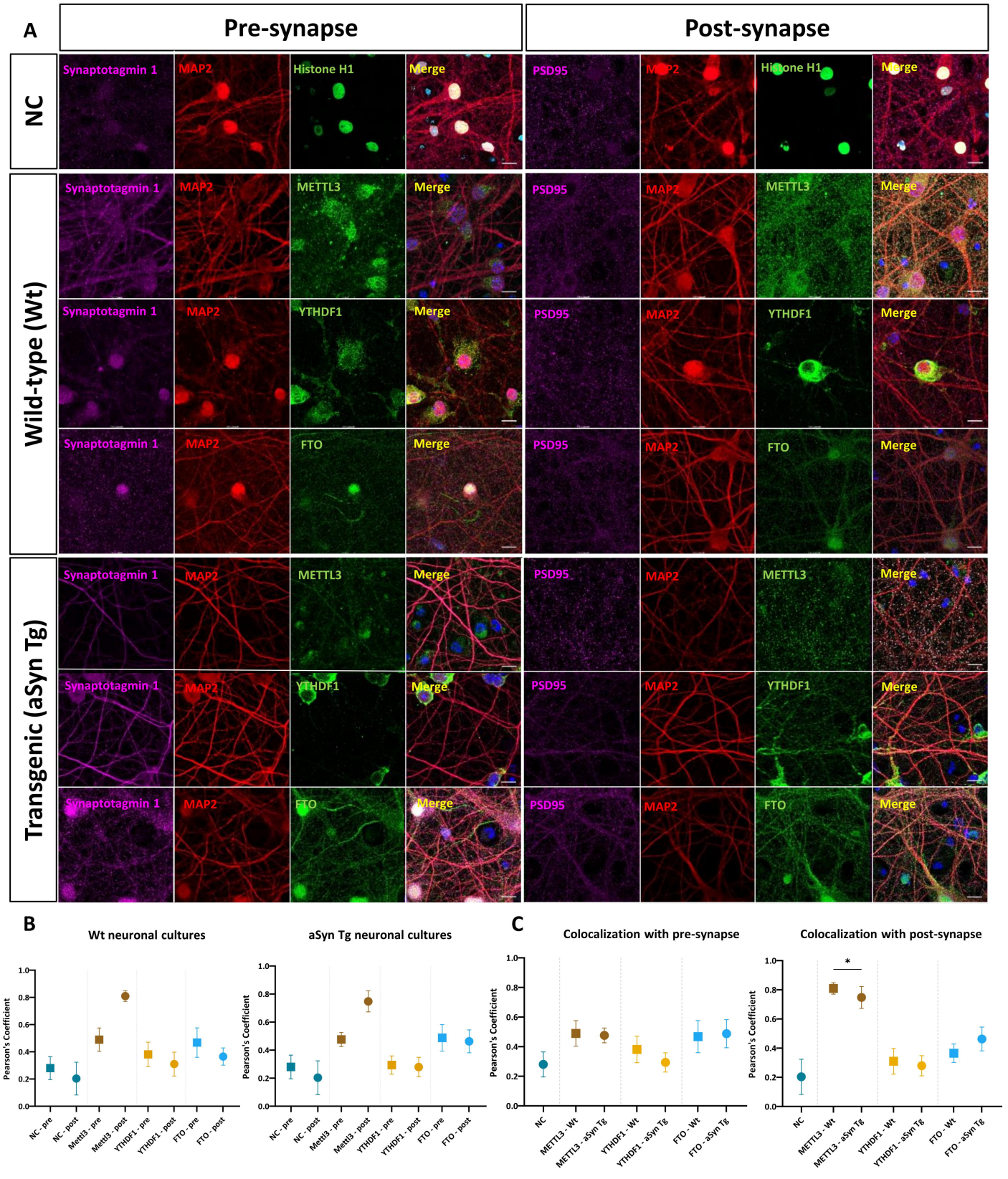
A
Pre-synapse
Post-synapse
NC
Wild-type (Wt)
Transgenic (aSyn Tg)
Synaptotagmin 1
MAP2
Histone H1
Merge
PSD95
METTL3
YTHDF1
FTO
B
Wt neuronal cultures
aSyn Tg neuronal cultures
Pearson's Coefficient
NC - pre
NC - post
Mettl3 - pre
Mettl3 - post
YTHDF1 - pre
YTHDF1 - post
FTO - pre
FTO - post
C
Colocalization with pre-synapse
Colocalization with post-synapse
NC
METTL3 - Wt
METTL3 - aSyn Tg
YTHDF1 - Wt
YTHDF1 - aSyn Tg
FTO - Wt
FTO - aSyn Tg
*

Figure 5.

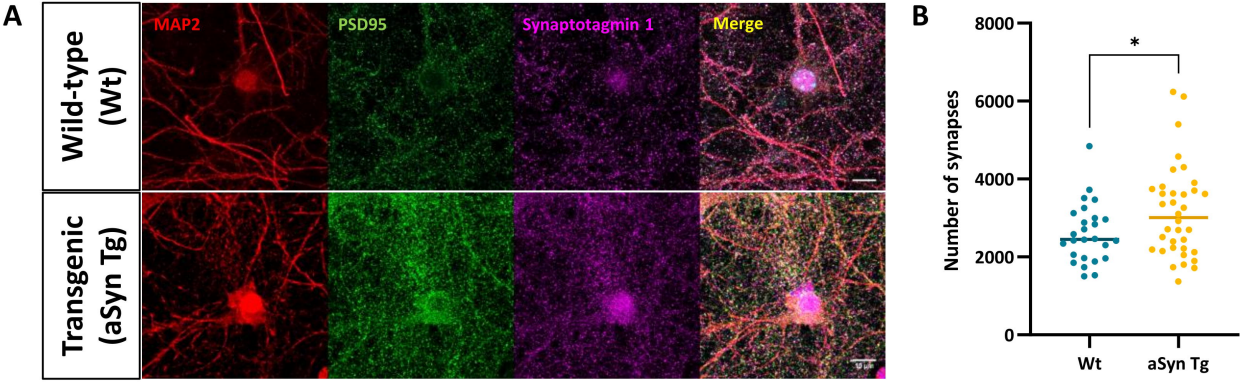
A
Wild-type (Wt)
Transgenic (aSyn Tg)
MAP2
PSD95
Synaptotagmin 1
Merge
B
Number of synapses
8000
6000
4000
2000
0
*
Wt
aSyn Tg

Figure 6.